Atmos. Chem. Phys. Discuss., 15, 7171–7238, 2015
www.atmos-chem-phys-discuss.net/15/7171/2015/
doi:10.5194/acpd-15-7171-2015


Atmospheric Chemistry and Physics Discussions



# Five-year flask measurements of long-lived trace gases in India

**X. Lin[1], N. K. Indira[2], M. Ramonet[1], M. Delmotte[1], P. Ciais[1], B. C. Bhatt[3], M. V. Reddy[4], D. Angchuk[3], S. Balakrishnan[4], S. Jorphail[3], T. Dorjai[3], T. T. Mahey[3], S. Patnaik[4], M. Begum[5], C. Brenninkmeijer[6], S. Durairaj[5], R. Kirubagaran[7], M. Schmidt[1,8], P. S. Swathi[2], N. V. Vinithkumar[5], C. Yver Kwok[1], and V. K. Gaur[2]**

[1]Laboratoire des Sciences du Climat et de l'Environnement (LSCE), UMR CEA-CNRS-UVSQ, Gif-sur-Yvette 91191, France
[2]CSIR Fourth Paradigm Institute (formerly CSIR Centre for Mathematical Modelling and Computer Simulation), NAL Belur Campus, Bangalore 560 037, India
[3]Indian Institute of Astrophysics, Bangalore 560 034, India
[4]Department of Earth Sciences, Pondicherry University, Puducherry 605 014, India
[5]Andaman and Nicobar Centre for Ocean Science and Technology (ANCOST), ESSO-NIOT, Port Blair 744103, Andaman and Nicobar Islands, India
[6]Max Planck Institute for Chemistry, Hahn-Meitner-Weg 1, 55128 Mainz, Germany
[7]Earth System Sciences Organisation – National Institute of Ocean Technology (ESSO-NIOT), Ministry of Earth Sciences, Government of India, Tamil Nadu, Chennai 600 100, India
[8]Institut für Umweltphysik, Universität Heidelberg, INF 229, 69120 Heidelberg, Germany







Received: 26 January 2015 – Accepted: 4 February 2015 – Published: 10 March 2015

Correspondence to: X. Lin (xin.lin@lsce.ipsl.fr)

Published by Copernicus Publications on behalf of the European Geosciences Union.





ACPD
15, 7171–7238, 2015



## Abstract

With the rapid growth in population and economic development, emissions of greenhouse gases (GHGs) from the Indian subcontinent have sharply increased during recent decades. However, evaluation of regional fluxes of GHGs and characterization of their spatial and temporal variations by atmospheric inversions remain uncertain due to a sparse regional atmospheric observation network. As a result of Indo-French collaboration, three new atmospheric stations were established in India at Hanle (HLE), Pondicherry (PON) and Port Blair (PBL), with the objective of monitoring the atmospheric concentrations of GHGs and other trace gases. Here we present the results of five-year measurements (2007–2011) of $CO_2$, $CH_4$, $N_2O$, $SF_6$, CO, and $H_2$ from regular flask sampling at these three stations. For each species, annual means, seasonal cycles and gradients between stations were calculated and related to variations in the natural GHG fluxes, anthropogenic emissions, and the monsoon circulations. Covariances between species at the synoptic scale were analyzed to investigate the dominant source(s) of emissions. The flask measurements of various trace gases at the three stations show potential to constrain the inversions of fluxes over Southern and Northeastern India. However, this network of ground stations needs further extension to other parts of India to allow a better understanding of, and constraints on the GHG budgets at regional and continental scales.

## 1 Introduction

Since the pre-industrial times, anthropogenic greenhouse gas (GHG) emissions have progressively increased the radiative forcing of the atmosphere, leading to impacts on the climate system and human society (IPCC, 2013, 2014a, b). With rapid socio-economic development and urbanization during the recent decades, a large and growing share of GHG emissions is contributed by emerging economies like China and India. In 2010, India became the world's third largest GHG emitter, next to China and the





ACPD
15, 7171–7238, 2015



USA (EDGAR v4.2; Le Quéré et al., 2014). Between 1991 and 2010, anthropogenic GHG emissions in India increased by ∼ 100 % from 1.4 to 2.8 Gt $CO_2$ eq (EDGAR v4.2). Without a systematic effort at mitigation, this trend would continue in the coming decades, given that the per capita emission rate in India is still much below that of the more developed countries (in 2010, the per capita GHG emission rates were 2.2, 10.9, 17.6, and 21.6 ton $CO_2$ eq/capita for India, the UK, Russia, and the USA, respectively; EDGAR v4.2). In particular, non-$CO_2$ GHG emissions are substantial in India, most of which are contributed by agriculture-related activities over populous rural areas (Pathak et al., 2010). In 2010, anthropogenic $CH_4$ and $N_2O$ emissions in India amounted to 29.6 Tg $CH_4$ (≈ 0.62 Gt $CO_2$ eq) and 0.8 Tg $N_2O$ (≈ 0.23 Gt $CO_2$ eq), together accounting for 32 % of the country's GHG emissions, of which contributions of the agricultural sector were 60 and 73 %, respectively (EDGAR v4.2). Reducing these two non-$CO_2$ GHG emissions possibly offers a cost-effective way to mitigate future climate change (Montzka et al., 2011).

Effective climate mitigation strategies need accurate monitoring and reporting of sources and sinks of GHGs. This is also a requirement of the United Nations Framework Convention on Climate Change (UNFCCC). Current estimates of GHG budgets in India, either from the top-down approach or bottom-up approach, have larger uncertainties than for other continents. For instance, Patra et al. (2013) reported a net biospheric $CO_2$ sink of $-104 \pm 150$ TgC $yr^{-1}$ over South Asia during 2007–2008 based on global inversions from 10 TransCom-$CO_2$ models (Peylin et al., 2013) and a regional inversion (Patra et al., 2011b), while the bottom-up approach gave an estimate of $-191 \pm 193$ TgC $yr^{-1}$ over the period of 2000–2009 (Patra et al., 2013). Notably, these estimates have uncertainties as high as 100–150 %. Evaluation of $N_2O$ emissions from 5 TransCom-$N_2O$ inversions also exhibited the largest differences over South Asia (Thompson et al., 2014b). A main source of uncertainty is the lack of atmospheric observation datasets with sufficient temporal and spatial coverage (Patra et al., 2013; Thompson et al., 2014b). Networks of atmospheric stations that were used to constrain estimates of global GHG fluxes show gaps over South Asia (Patra et al., 2011a;





ACPD
15, 7171–7238, 2015



Thompson et al., 2014b, c; Peylin et al., 2013), with Cape Rama (CRI) on the southwest coast of India being the only Indian station (Rayner et al., 2008; Patra et al., 2009; Tiwari et al., 2011; Bhattacharya et al., 2009; Saikawa et al., 2014). Although recent aircraft and satellite observations have provided useful constraints on estimates of regional GHG fluxes (Park et al., 2007; Xiong et al., 2009; Schuck et al., 2010; Patra et al., 2011b; Niwa et al., 2012; Zhang et al., 2014), a denser atmospheric observational network is needed over this region for an improved, more detailed, and necessary understanding of sources and sinks of GHGs.

Besides a lack of observation sites, the seasonally reversing Indian monsoon circulations and orographic effects complicate simulation of regional atmospheric transport, which contributes to uncertainty of the inverted GHG fluxes (e.g., Thompson et al., 2014b). The Indian monsoon system is a prominent meteorological phenomenon in South Asia, which, at lower altitudes, is characterized by strong southwesterlies from the Arabian Sea to the Indian subcontinent during the boreal summer, and northeasterlies during the boreal winter (Goswami, 2005). The summer monsoon is associated with deep convection, which mixes the boundary layer air into the upper troposphere and lower stratosphere (Schuck et al., 2010; Lawrence and Lelieveld, 2010). The Indian monsoon also impacts biogenic activities (e.g., vegetation growth, microbial activity) and GHG fluxes through its effects on rainfall variations (Tiwari et al., 2013; Valsala et al., 2013; Gadgil, 2003). Given that accurate atmospheric transport is critical to retrieve accurate inversion of GHG fluxes, an observational network that comprises a range of altitudes (including monitoring stations in mountainous regions) is valuable for validating and improving atmospheric transport models.

Since the 2000s, three new atmospheric ground stations have been established in India as part of Indo-French collaboration, aiming to monitor GHGs and other trace gases in flask air samples. Of the three Indian stations, Hanle (HLE) is a high-altitude station situated in the western Indian Himalayas, while Pondicherry (PON) and Port Blair (PBL) are tropical surface stations located respectively on the southeastern coast of South India and on an oceanic island in the southeastern Bay of Bengal. In this





ACPD
15, 7171–7238, 2015



study, we briefly describe main aspects of the stations and present time series of flask air sample measurements of multiple trace gases at HLE, PON, and PBL over the period 2007–2011. Descriptions of the three stations as well as methods used to analyze and calibrate the flask measurements are given in Sect. 2. For each station, four GHG species ($CO_2$, $CH_4$, $N_2O$, $SF_6$) and two additional trace gases (CO, $H_2$) are measured to characterize the annual means and seasonal cycles, with results and discussions presented in Sect. 3. Gradients between different stations are interpreted in the context of regional flux patterns and monsoon circulations (Sect. 3.1). We also analyze covariances between species (using deviations from their smoothed fitting curves) for synoptic variations (Sect. 3.2). Finally, we investigate two abnormal $CH_4$ and CO events at PBL and propose likely sources and origins (Sect. 3.3). We summarize the paper and draw conclusions in Sect. 4.

## 2 Sampling stations and methods

### 2.1 Sampling stations

Figures 1 and S1 in the Supplement show the locations of HLE, PON, and PBL. We also present five-day back-trajectories from each station for all sampling dates in April–June (AMJ; Fig. 1a), July–September (JAS; Fig. 1b), October–December (OND; Fig. 1c) and January–March (JFM; Fig. 1d), respectively. Note that this four-period classification scheme is slightly different from the climatological seasons defined by India Meteorological Department (IMD; Attri and Tyagi, 2010), in which months of a year are categorized into the pre-monsoon season (March–May), SW monsoon season (June–September), post-monsoon season (October–December) and winter season (January and February). We adapted the IMD classification to facilitate better display and further analyses (e.g., Sect. 3.2), making sure that samples are fairly evenly distributed across all seasons. The back-trajectories were generated using the Hybrid Single Particle Lagrangian Integrated Trajectory (HYSPLIT4) model (Draxler and





ACPD
15, 7171–7238, 2015



Rolph, 2003), driven by wind fields from the Global Data Assimilation System (GDAS) archive data based on National Centers for Environmental Prediction (NCEP) model output (https://ready.arl.noaa.gov/gdas1.php).

The Hanle (HLE) station (32.78° N, 78.96° E, 4517 m a.s.l.) is located in the campus of the Indian Astronomical Observatory (IAO) atop Mt. Saraswati, about 300 m above the Nilamkhul Plain in the Hanle Valley of southeastern Ladakh in northwestern Himalayas. The station was established in 2001 as a collaborative project with the Indian Institute of Astrophysics. The area around the station is a cold mountain desert, with sparse vegetation and a small population of ~ 1700 distributed over an area of ~ 20 $km^2$. Anthropogenic activities are limited to small-scale crop production (e.g., barley and wheat) and livestock farming (e.g., yaks, cows, goats, and sheep). The nearest populated, industrialized city of Leh (34.25° N, 78.00° E, 3480 m a.s.l.) with ~ 27 000 inhabitants, lies 270 km to the northwest of this station. By virtue of its remoteness, high altitude, and negligible biotic and anthropogenic influences, HLE is representative of background free tropospheric air masses in the mid-latitude of Northern Hemisphere. Regular flask air sampling has been operational since February 2004, and in-situ $CO_2$ measurements started in September 2005 (Ramonet et al., 2015). Over the period 2007–2011, a total of 188 flask sample pairs were collected at HLE. Back-trajectories show that, HLE dominantly sampled air masses that pass over northern Africa and the Middle East throughout the year, and those coming from South and Southeast Asia during the SW monsoon season (Fig. 1). More detailed station information of HLE would be found in several earlier publications (Babu et al., 2011; Moorthy et al., 2011).

The Pondicherry (PON) station (12.01° N, 79.86° E, 20 m a.s.l.) is located on the southeast coast of India, about 8 km north of the city of Pondicherry with a population of ~ 240 000 (Census India, 2011). The station was established in collaboration with Pondicherry University in 2006. The flask sampling inlet was initially located on a 10 m mast fixed on the roof of the University Guest House, later moved to a 30 m high tower in June 2011. The surrounding village Kalapet, has a population of ~ 9000 (Sivakumar and Anitha, 2012). A four-lane highway runs nearly 80 m to the west of the station,





ACPD
15, 7171–7238, 2015



while the Indian Ocean stands about 100 m to the east of the station. Moreover, the two nearest megalopolises of Chennai and Bangalore, both with populations of over 4 million (Census India, 2011), are approximately 120 km to the north and 260 km to the west of the station. In order to minimize the influences of local GHG sources/sinks, flask air sampling at PON is performed between 12:00 and 18:00 local time (LT), when the sea breeze moves clean air masses towards the land and the boundary layer air is well mixed. Flask sampling began in September 2006. Over the period 2007–2011, a total of 185 flask sample pairs were collected at PON. As shown in Fig. 1, the air masses received at PON are strongly related to the monsoon circulations. During the boreal summer when the southwest monsoon prevails, PON is influenced by air masses originating from the Arabian Sea and South India, whereas during the boreal winter, it receives air masses from the east and northeast parts of the Indian subcontinent, and the Bay of Bengal. During the boreal spring and autumn when the monsoon changes its direction, air masses of both origins are observed.

The Port Blair (PBL) station (11.65° N, 92.76° E, 20 m a.s.l.) is located on the small Andaman Islands in the southeastern Bay of Bengal, ~ 1400 km east of Pondicherry, and roughly 600 km west of Myanmar and Thailand. The station was established in collaboration with the National Institute of Ocean Technology (NIOT), India, and flask air sampling was initiated in July 2009. The main city on the Andaman Islands, Port Blair, is about 8 km to the north of the station, with a population of ~ 100 000 (Census India, 2011). Due to its proximity to vegetation and a small rural community, the station is not completely free from influences of local GHG fluxes. Therefore, flask samples at PBL are obtained in the afternoon between 13:00 and 15:00 LT, when the sea breeze moves towards the land, to minimize significant local influences. Over the period 2009–2011, a total of 63 flask sample pairs were collected at PBL. Back-trajectories show that the air masses sampled at PBL are also controlled by the seasonally reversing monsoon circulations (Fig. 1), with air masses from the Indian Ocean south of the Equator during the southwest monsoon season, and from the northeast part of the Indian subcontinent, the Bay of Bengal, and Southeast Asia during the northeast monsoon season.





ACPD
15, 7171–7238, 2015



As for PON, air masses of both origins are detected at PBL during the boreal spring and autumn when the monsoon changes its direction.

## 2.2 Flask sampling and analysis

### 2.2.1 Flask sampling

In principle, flask samples are taken in pairs on a weekly basis at all three stations. However, in practice air samples are collected less frequently (on average every 10–12 days) due to bad meteorological conditions or technical problems. Whole air samples are filled into pre-conditioned 1 L cylindrical borosilicate glass flasks (Normag Labor und Prozesstechnik GmbH, Germany) with KEL-F (PTCFE) valves (Glass Expansion, Australia or Normag, Germany) fitted at both ends. Besides, flasks equipped with the original Teflon PFA O-ring valves are also used ($\sim$ 5.0, 1.2 and 1.1 % of air samples for HLE, PON and PBL during the study period, respectively), and a storage correction for the loss of $CO_2$ ($+0.0027\,ppm\,day^{-1}$) and of $N_2O$ ($+0.0035\,ppb\,day^{-1}$) is applied after analyses of the samples. The correction factors are empirically determined based on laboratory storage tests using flasks filled with calibrated gases. Drying of the air is performed using 10 g of magnesium perchlorate ($Mg(ClO_4)_2$) confined at each end with a glass wool plug in a stainless steel cartridge, located upstream of the pump unit. To prevent entrainment of material inside the sampling unit, a 7 µm filter is attached at the end of the cartridge. The flasks are flushed prior to the sampling for 10–20 min at a rate of 4–5 $L\,min^{-1}$, and the air is compressed in the flasks to about 1 bar over ambient pressure (pump: KNF Neuberger diaphragm pump powered by a 12V DC motor, Germany, N86KNDC with EPDM membrane). The pressurizing process lasts for less than a minute.





ACPD
15, 7171–7238, 2015



### 2.2.2 Flask analyses

On average the flasks arrive at LSCE, France about 150 days after the sampling date, and are analyzed for $CO_2$, $CH_4$, $N_2O$, $SF_6$, CO, and $H_2$ with two coupled gas chromatograph (GC) systems. The first gas chromatograph (HP86890, Agilent) is equipped with a flame ionization detector (FID) for $CO_2$ and $CH_4$ detection, and an electron capture detector (ECD) for $N_2O$ and $SF_6$ detection. It is coupled with a second GC equipped with a reduced gas detector (RGD, Peak Laboratories, Inc., California, USA), for analyzing CO and $H_2$ via reduction of HgO and subsequent detection of Hg vapor through UV absorption (Lopez et al., 2012; Yver et al., 2009).

Both GC systems are composed of three complementary parts: the injection device, the separation elements and the detection sensors. As flask samples are already dried during sampling, they are only passed through a 5 mL glass trap maintained in an ethanol bath kept at −55 °C by a cryocooler (Thermo Neslab CC-65) to remove any remaining water vapor. The air samples are flushed through a 15 mL sample loop for $CO_2$ and $CH_4$ analyses, a 10 mL sample loop for $N_2O$ and $SF_6$ analyses, and a 1 mL sample loop for CO and $H_2$, at a flow rate of 200 mL min$^{-1}$. After temperature and pressure equilibration, the sampled air is injected into the columns. For $CO_2$ and $CH_4$ separation, a Hayesep-Q ($12' \times 3/16''$ SS, mesh 80/100) analytical column is used. For $N_2O$ and $SF_6$ separation, a pre-column with Hayesep-Q ($4' \times 3/16''$ SS, mesh 80/100) and an analytical column with Hayesep-Q ($6' \times 3/16''$ SS, mesh 80/100) are used. Detection of $CH_4$ and $CO_2$ (after conversion to $CH_4$ using a Nickel catalyst and $H_2$ gas) is performed in the FID. The temperature of the FID is kept at 300 °C and the flame is fed with $H_2$ (provided by a NM-$H_2$ generator from F-DBS) at a flow rate of 65 mL min$^{-1}$ and zero air (provided by a 75–82 zero air generator from Parker–Balston) at a flow rate of 400 mL min$^{-1}$. Detection of $N_2O$ and $SF_6$ is performed in the ECD. For CO and $H_2$, we use a pre-column (Unibeads 1S mesh 60/80; 1/8 inches OD × 16.5 inches) to separate the two gases from the air matrix, and use an analytical column (Molecular Sieve 5° A mesh 60/80; 1/8 inches CD × 80 inches) to effectively separate





ACPD
15, 7171–7238, 2015



$H_2$ from CO, both of which are analyzed in the RGD detector. A measurement takes ~ 5 min and calibration gases are measured at least every 0.45 h. For $CO_2$, $CH_4$, $N_2O$, and $SF_6$, we use two calibration gases, one with a high concentration and the other with a low concentration. The concentration of the sample is calculated using a linear regression between the two calibration gases with a time interpolation between the two measurements of the same calibration gas (Messager, 2007; Lopez, 2012). For CO and $H_2$, we use only one standard and apply a correction for the non-linearity of the analyzer (Yver et al., 2009; Yver, 2010). The nonlinearity is verified regularly with 5 calibration cylinders for CO and 8 calibration cylinders for $H_2$. All the calibration gases themselves are determined against an international primary scale (Dlugokencky et al., 2005; Zhao and Tans, 2006; Jordan and Steinberg, 2011; Hall et al., 2007). Finally, a "target" gas is measured every two hours after the calibration gases as a quality control of the scales and of the analyzers. The repeatability of the GC systems estimated from the target cylinder measurements over several days is 0.06 ppm for $CO_2$, 1 ppb for $CH_4$, 0.3 ppb for $N_2O$, 0.1 ppt for $SF_6$, 1 ppb for CO and 2 ppb for $H_2$. Additional quality control is made by checking values of a flask target (a flask filled with calibrated gases) placed on each measurement sequence.

For both of the GC systems, data acquisition, valve shunting, and temperature regulation are entirely processed by the Chemstation software from Agilent. Concentrations are calculated with a software developed at LSCE using peak height or area depending on the species. More detailed descriptions of flask analysis are available in Yver et al. (2009) and Lopez et al. (2014).

### 2.2.3 Uncertainty of flask measurements

Uncertainties in the measured concentrations stem from both the sampling method and the analysis. Collecting flask samples in pairs and measuring each flask twice allow us to evaluate these uncertainties. A large discrepancy between two analyses of the same flask reveals a problem in the analysis system, while a difference between a pair of flasks reflects both analysis and sampling uncertainties. Flask pairs with differences





ACPD
15, 7171–7238, 2015



in mole fractions beyond a certain threshold are flagged and rejected (see Table S2 in the Supplement for the threshold for each species). The percentages of retained flask pairs after flagging amount to 65.9–88.3 % for $CO_2$, 88.6–94.1 % for $CH_4$, 74.6–91.5 % for $N_2O$, 92.0–96.8 % for $SF_6$, 68.6–88.3 % for CO, and 76.2–95.2 % for $H_2$ (Table S3). For each species, we evaluate the uncertainties by averaging differences between the two injections of the same flask (analysis uncertainty) and between the pair of flasks (analysis uncertainty + sampling uncertainty) across all retained flask pairs from the three Indian stations (Table S4). For all species except $SF_6$, the sampling uncertainty turns out to be the major uncertainty, while the analysis uncertainty is equivalent to the reproducibility of the instrument. For $SF_6$, both uncertainties are extremely low due to the small amplitudes and variations of the signals at the three stations.

Finally, all results are linked to the international scales defined for each species ($CO_2$: WMOX2007; $CH_4$: NOAA2004; $N_2O$: NOAA2005A; $SF_6$: NOAA2005; CO: WMOX2004; $H_2$: WMOX2009). In the GC systems, the flask samples are measured against a secondary scale which is regularly calibrated against the primary scale maintained at LSCE (Hall et al., 2007; Dlugokencky et al., 2005; Jordan and Steinberg, 2011; Zhao and Tans, 2006). At LSCE, there are regular comparison exercises in which flasks are measured by different laboratories on the same primary scale (e.g., Inter-Comparison Project (ICP) loop, Integrated non-$CO_2$ Greenhouse gas Observing System (InGOS) "Cucumber" intercomparison project). These comparisons allow us to estimate possible biases in our measurements. In Table S4, the bias for each species is calculated over the sampling period using the ICP flask exercise that circulates flasks of low, medium and high concentrations between different laboratories. For $CO_2$, $CH_4$, $SF_6$ and CO, the biases are reported against NOAA (NOAA-LSCE) as it is the laboratory responsible for the primary scales for these species. The bias of $H_2$ is calculated against Max Planck Institute for Biogeochemistry (MPI-BGC) in Jena, Germany, which is responsible for the primary scale of $H_2$. The bias of $N_2O$ is reported against MPI-BGC instead of NOAA. Although NOAA is responsible for the primary scale of $N_2O$, the instruments they use for the $N_2O$ flask analyses and cylinder calibration are not the





ACPD
15, 7171–7238, 2015



same as ours. For $CH_4$, $N_2O$, $SF_6$ and $H_2$, the estimated biases are within the noise of the instrument and negligible. For $CO_2$ and CO, we observe a bias of $-0.15 \pm 0.11$ and $3.5 \pm 2.2$ ppb, respectively (Table S4), which could be due to the nonlinearity of the instrument and/or an improper attribution of the secondary scale values.

## 2.3 Data analyses

### 2.3.1 Curve-fitting procedures

For each time series of flask measurements, we calculated annual means and seasonal cycles using a curve-fitting routine (CCGvu) developed by NOAA/CMDL (Thoning et al., 1989). A smoothed function was fitted to the retained data, consisting of a first-order polynomial for the growth rate and two harmonics for the annual cycle (Levin et al., 2002; Ramonet et al., 2002), as well as a low pass filter with 80 and 667 days as short-term and long-term cutoff values, respectively (Bakwin et al., 1998). Residuals were then calculated as the differences between the original data and the smoothed fitting curve. Any data lying outside three standard deviations of the residuals were regarded as outliers and also discarded from the time series (Harris et al., 2000; Zhang et al., 2007). This procedure was repeated until no outliers were identified. The data discarded through this filtering procedure accounts for less than 4 % of the retained flask pairs after flagging (Table S3). The annual means, as well as the amplitude and phases of seasonal cycles, were determined from the smoothed fitting curve and its harmonic component. We bootstrapped the curve-fitting procedures 1000 times by randomly sampling the original data with replacement to further estimate uncertainties of annual means and seasonal cycles. Since the observation records are relatively short, we used all flask measurements between 2006 and 2011 to fit the smooth curve when available (Fig. S2). For each species, we also compared results with measurements from stations outside India that belong to other networks (e.g., NOAA/ESRL and Integrated Carbon Observation System (ICOS)). Locations and the fitting periods of these stations are also given in Table S1, Figs. S1 and S2.





ACPD
15, 7171–7238, 2015



### 2.3.2 Ratio of species

We analyzed $CH_4$-CO, $CH_4$-$CO_2$, and CO-$CO_2$ correlations using the residuals from the smoothed fitting curves that represent synoptic-scale variations (Harris et al., 2000; Ramonet et al., 2002; Grant et al., 2010). As in previous studies, we used slopes calculated from the orthogonal distance regression as ratios between species to equally account for variances of both species (Harris et al., 2000; Ramonet et al., 2002; Schuck et al., 2010; Baker et al., 2012).

## 3 Results and discussions

### 3.1 Annual means and seasonal cycles

#### 3.1.1 $CO_2$

Figure 2 shows $CO_2$ flask measurements and the corresponding smooth curves fitted to the data at HLE, PON and PBL, as well as two additionally NOAA/ESRL stations, namely Plateau Assy, Kazakhstan (KZM – 43.25° N, 77.88° E, 2519 m a.s.l.) and Waliguan, China (WLG – 36.29° N, 100.90° E, 3810 m a.s.l.) (Dlugokencky et al., 2014b). HLE observed an increase in $CO_2$ mole fractions from 382.3±0.3 to 391.4±0.3 between 2007 and 2011, with annual mean values being lower (by 0.2–1.9 ppm) than KZM and WLG (Fig. 2c and d, Table 1). At PON, the annual mean $CO_2$ mole fractions were generally higher than at HLE, with differences ranging 1.8–4.3 ppm (Fig. 2a, Table 1). The annual mean $CO_2$ gradient between PON and HLE reflects the altitudinal difference of the two stations, and a larger influence of $CO_2$ emissions at PON, mostly from South India (Fig. 1, EDGAR v4.2). Besides this, as shown in Fig. 2a and Table 1, the $CO_2$ observations at PON are influenced by local and synoptic scale events, with a large variability of individual measurements relative to the fitting curve (see the relative SDs (RSD) in Table 1). At PBL, the annual mean $CO_2$ mole fractions were on





ACPD
15, 7171–7238, 2015



average 1.2–1.8 ppm lower than that at HLE (Table 1). The negative gradient between PBL and HLE is particularly large during summer, possibly due to clean air masses transported from the ocean (Figs. 1 and 2b). Note that caution should be exercised in interpreting the gradient at PBL because of the data gap and short duration of the time series.

The different $CO_2$ seasonal cycles observed at the five stations reflect the seasonality of carbon exchange in the northern terrestrial biosphere as well as influences of long-range transport and the monsoon circulations. At HLE, the peak-to-peak amplitude of the mean seasonal cycle was $8.2 \pm 0.4$ ppm, with the maximum early May and the minimum mid-September, respectively (Fig. 3, Table 1). The mean seasonal cycle estimated from flask measurements at HLE is in good agreement with that derived from vertical profiles of in-situ aircraft measurements over New Delhi (~ 500 km southwest of HLE) from the Comprehensive Observation Network for Trace gases by Airliner (CONTRAIL) project at similar altitudes (Fig. 3a; Machida et al., 2008), confirming that HLE is representative of regional free mid-troposphere background concentrations. When comparing with the two other background stations located further north in central and East Asia, a significant delay of the $CO_2$ phase is seen at HLE compared to KZM and WLG (Fig. 3b, Table 1). We also note that the $CO_2$ mean seasonal cycle at HLE is in phase with the composite zonal marine boundary layer (MBL) reference at 32° N, while for KZM and WLG, an advance in the $CO_2$ phase by about 1 month is observed compared to the zonal MBL reference (Fig. S3; Dlugokency et al., 2014b). The phase shifts in the $CO_2$ seasonal cycles mainly result from differences in air mass origins between stations. HLE is influenced by the long-range transport of air masses from mid-latitudes around 30° N, as well as air masses passing over the Indian subcontinent in the boreal summer (Fig. 1), therefore its $CO_2$ seasonal cycle is related to the seasonality of vegetation activity over the entire latitude band. KZM and WLG receive air masses passing over the Middle East and western Asia as HLE does, but they are also influenced by air masses of more northern origins with signals of strong $CO_2$ uptake over Siberia during JAS (Fig. S4). At WLG, negative $CO_2$ synoptic events, indicative





ACPD
15, 7171–7238, 2015



of large-scale transport of air masses exposed to carbon sinks in Siberia in summer, were also detected by in-situ measurements during 2009–2011 (Fang et al., 2014). Moreover, the back-trajectories indicate that WLG and KZM are more influenced than HLE by air masses that have exchanged with the boundary layer air being affected by vegetation $CO_2$ uptake (Fig. S5a, d, e). This could additionally account for the earlier $CO_2$ phase observed at KZM and WLG compared to HLE.

At PON and PBL, the $CO_2$ mean seasonal cycle is controlled by changes in the monsoon circulations, in combination with the seasonality of $CO_2$ biotic exchange and anthropogenic emissions in India. During the boreal winter when the NE monsoon prevails, PON and PBL receive air masses enriched in $CO_2$ from the East and Northeast Indian subcontinent as well as from Southeast Asia, with large anthropogenic $CO_2$ emissions (EDGAR v4.2; Wang et al., 2013; Kurokawa et al., 2013). During April when the SW monsoon begins to develop, the two stations record a decrease in $CO_2$ because of the arrival of air masses depleted in $CO_2$ originating from the Indian Ocean south of the Equator (Fig. 1, Fig. 3c). Compared to PBL, the $CO_2$ decrease at PON is less pronounced and longer, probably because of the influence of anthropogenic emissions in South India.

### 3.1.2 $CH_4$

Figure 4 presents time series of $CH_4$ flask measurements at the three Indian stations and the two NOAA/ESRL stations (Dlugokencky et al., 2014a), with their corresponding smoothed curves for 2007–2011. At HLE, annual mean $CH_4$ increased from 1814.8 ± 2.9 to 1849.5 ± 5.2 ppb between 2007 and 2011 (Fig. 4, Table 1). The multiyear mean $CH_4$ value at HLE was lower than at KZM and WLG by on average 25.7±3.1 and 19.6± 7.8 ppb (Fig. 4c and d, Table 1), respectively, reflecting the latitudinal and altitudinal $CH_4$ gradients. Indeed, KZM and WLG receive air masses transported from Siberia with large wetland $CH_4$ emissions in summer (Fig. S4), which further contribute to the positive gradients between the two stations and HLE. At PON and PBL, the annual mean $CH_4$ mole fractions were higher than at HLE by as much as 37.4±10.7 and 19.8±





ACPD
15, 7171–7238, 2015



24.5 ppb respectively (Fig. 4a and b, Table 1). The positive gradients indicate significant regional $CH_4$ emissions, especially during winter when the NE monsoon transports air masses from East and Northeast India and Southeast Asia, where emissions from livestock, rice paddies and a variety of waterlogged anaerobic sources and residential biofuel burning are intense (EDGAR v4.2; Baker et al., 2012; Kurokawa et al., 2013).

The $CH_4$ seasonal cycles exhibit contrasting patterns across stations. As shown in Fig. 5, a distinct characteristic of the mean seasonal cycle at HLE is a $CH_4$ maximum from June to September. Even KZM and WLG do not show a minimum in summer that would be characteristic for the enhanced $CH_4$ removal rate by reaction with OH. The pronounced HLE feature is consistent with the result from the aircraft flask measurements over India at flight altitudes of 8–12.5 km by the Civil Aircraft for the Regular Investigation of the atmosphere Based on an Instrument Container (CARIBIC) project (Schuck et al., 2010, 2012; Baker et al., 2012), although an apparent phase shift (lag by one month) and a larger seasonal cycle amplitude are found in the CARIBIC composite data due to vertical mixing between the mid- and upper troposphere (Fig. 5a). Apparently, CARIBIC sampled the mid- to upper tropospheric air masses that were earlier and more strongly enriched in $CH_4$ due to the rapid uplift in regions of strong convection. Xiong et al. (2009) also reported enhancement of $CH_4$ during the summer monsoon season over South Asia based on satellite retrievals of $CH_4$ using the Atmospheric Infrared Sounder (AIRS) on the EOS/Aqua platform as well as model simulations. Moreover, the mean $CH_4$ seasonal cycle at HLE agrees well with the annual variation of convective precipitation over the Indian subcontinent (Fig. 5b), which is derived from ECMWF nudged Laboratoire de Météorologie Dynamique general circulation model (LMDz) (Hauglustaine et al., 2004). This agreement indicates that the summer maximum at HLE can be attributed to the enhanced biogenic $CH_4$ emissions from wetlands and rice paddies and deep convection that mixes surface emissions into the mid-to-upper troposphere. During the SW monsoon period (June–September), convection over the Indian subcontinent and the Bay of Bengal rapidly mixes surface polluted air with the upper troposphere, thereby enhancing concentrations of trace gases





ACPD
15, 7171–7238, 2015



(Schuck et al., 2010; Lawrence and Lelieveld, 2010). As stated above, KZM and WLG also record $CH_4$ increases during summertime, but with smaller magnitudes (Fig. 5a), since they are not directly influenced by deep convection from the Indian monsoon system.

At PON and PBL, in contrast to HLE, the $CH_4$ mean seasonal cycles have distinct phases and much larger amplitudes, with minimum $CH_4$ values during July (Fig. 5b). This not only reflect higher rates of removal by OH, but rather the influence of southern hemispheric air transported at low altitude from the Southwest as well as the dilution effect by increased local planetary boundary layer height. Since these air masses do not collect additional $CH_4$ from the various surface sources, they remain depleted in $CH_4$. In winter, the maxima at PON and PBL are associated with $CH_4$-enriched air masses transported from East and Northeast India, and Southeast Asia, mostly polluted by agricultural-related sources (e.g., livestock, rice paddies, agricultural waste burning).

### 3.1.3 $N_2O$

Time series of $N_2O$ flask measurements over the period of 2007–2011 and their smoothed curves are presented in Fig. 6. At HLE, the annual mean $N_2O$ rose from $322.2 \pm 0.1$ to $325.2 \pm 0.1$ ppb during 2007–2011 (Table 1), with a mean annual growth rate of $0.8 \pm 0.0$ ppb yr$^{-1}$ ($r^2 = 0.97$, $p = 0.001$). At PON and PBL, the annual mean $N_2O$ mole fractions are higher than at HLE by $3.1 \pm 0.3$ and $3.8 \pm 1.7$ ppb (Fig. 6, Table 1), respectively. The $N_2O$ gradients between PON, PBL and HLE are larger than typical $N_2O$ gradients observed between stations scattered in Europe or in North America. For example, Haszpra et al. (2008) presented $N_2O$ flask measurements at a continental station – Hegyhátsál, Hungary (HUN – 46.95° N, 16.65° W, 248 m a.s.l.) from 1997 to 2007. The annual mean $N_2O$ mole fraction at HUN was higher than at Mauna Loa (MLO) and Mace Head (MHD) by only 1.6 and 1.3 ppb, respectively. We also analyze $N_2O$ time series of flask measurements during 2007–2011 at several European coastal stations – BGU in Spain, FIK in Greece, and LPO in France (Table S1), and the $N_2O$ gradients between these stations and MHD were $1.1 \pm 0.2$, $0.4 \pm 0.1$, and $2.1 \pm 0.6$ ppb,





ACPD
15, 7171–7238, 2015



respectively (Fig. S7, Table S5). In the United States, $N_2O$ flask measurements from the NOAA/ESRL stations at Park Falls, Wisconsin (LEF – 45.95° N, 90.27° W, 472 m a.s.l.), Harvard Forest, Massachusetts (HFM – 42.54° N, 72.17° W, 340 m a.s.l.) and a continental, high-altitude station at Niwot Ridge, Colorado (NWR – 40.05° N, 105.58° W, 3523 m a.s.l.) also show that, the annual mean $N_2O$ concentrations at HFM and LEF were higher than that at NWR by only $0.5 \pm 0.1$ and $0.3 \pm 0.1$ ppb, respectively (Fig. S7, Table S5). Besides, the $N_2O$ concentrations measured at PON and PBL have a notably higher variability (around the smoothed fitting curve) than that at European and US stations (see relative SDs (RSD) in Table 1 and Table S5). The larger $N_2O$ gradient between PON, PBL and HLE, as well as higher variability at PON and PBL, demonstrate the presence of substantial $N_2O$ sources in South Asia and over the Indian Ocean during the observation period, related to emissions from natural and cultivated soils probably enhanced by extensive use of nitrogen fertilizers, as well as emissions in regions of coastal upwelling in the Arabian Sea (Bange et al., 2001; Garg et al., 2012; Saikawa et al., 2014).

Compared to $CO_2$ and $CH_4$, the seasonal cycle of $N_2O$ is very small due to the long lifetime of ~ 120 years (Minschwaner et al., 1993; Volk et al., 1997), and more noisy due to regional sources and synoptic variability. At HLE, PON and PBL, the peak-to-peak amplitudes of the $N_2O$ seasonal cycle are $0.6 \pm 0.1$, $1.2 \pm 0.5$, and $2.2 \pm 0.6$ ppb, respectively (Table 1). HLE displays a $N_2O$ maximum in mid-August (Student's $t$ test, $t = 1.78$, $p = 0.06$), and a secondary maximum is in January/February but not significant (Student's $t$ test, $t = -0.84$, $p = 0.79$) (Table 1, Fig. 7, Table S6 for detailed $t$ test statistics). The $N_2O$ seasonal cycle at HLE is out of phase with that at other northern background stations such as MHD (Fig. S8, Table S5), where an $N_2O$ summer minimum is always observed, attributed to the downward transport of $N_2O$-depleted air from the stratosphere to the troposphere during spring and summer (Liao et al., 2004; Morgan et al., 2004; Jiang et al., 2007b). The timing of the summer $N_2O$ maximum at HLE is consistent with that of $CH_4$ (Table 1; Figs. 5 and 7), giving evidence that the $N_2O$ seasonal cycle is influenced by the convective mixing of surface air, rather than by the influx of





ACPD
15, 7171–7238, 2015



stratospheric air into the troposphere. Given that the populous Indo-Gangetic plains have high $N_2O$ emission rates due to intensive nitrogen fertilizer use (Garg et al., 2012; Thompson et al., 2014a), during summer, the surface air enriched in $N_2O$ is vertically transported by deep convection and enhances $N_2O$ mole fractions in the mid-to-upper troposphere. Like $CH_4$, the $N_2O$ enhancement at HLE during the summer monsoon period (June–September) is consistent with the aircraft flask measurements at flight altitudes 8–12.5 km from the CARIBIC project during April–December 2008 (Schuck et al., 2010).

At PON, $N_2O$ also decreases during February–April and reaches a minimum at the end of May. However, the decrease of $N_2O$ does not persist during June–September, which is in contrast with $CH_4$ (Table 1, Fig. 7a). One reason may be that the air masses transported by the SW monsoon do not collect substantial amounts of $CH_4$, but $N_2O$. The increase of $N_2O$ at PON during June–August and the maximum during September–October are likely related to $N_2O$ emissions from coastal upwelling along the southern Indian continental shelf, which peak during the SW monsoon season (Patra et al., 1999; Bange et al., 2001). According to Bange et al. (2001), the annual $N_2O$ emission for the Arabian Sea is 0.33–0.70 $Tg\,yr^{-1}$, of which $N_2O$ emissions during the SW monsoon account for about 64–70 %. This coastal upwelling $N_2O$ flux is significantly larger than the annual anthropogenic $N_2O$ emissions in South India south of 15° N, which is estimated to be on average 0.07–0.08 $Tg\,yr^{-1}$ during 2000–2010 (EDGAR v4.2). At PBL, the maximum and minimum $N_2O$ occur in November and February/March, respectively (Table 1, Fig. 7b). The late $N_2O$ peak at PBL in November may be associated with the $N_2O$-enriched air masses transported from South and Southeast Asia, which could be attributed to natural and agricultural $N_2O$ emissions from this region (Saikawa et al., 2014). It should be noted that, the mean seasonal cycles of $N_2O$ at PON and PBL are subject to high uncertainties because of the short observation periods and data gaps (shaded area in Fig. 7). The $N_2O$ maximum and/or minimum obtained from the mean seasonal cycle are marginally significant for PON and PBL (Table S6 for detailed *t* test statistics). Therefore, caution should be exercised





ACPD
15, 7171–7238, 2015



in interpreting mean seasonal cycles at these stations. Sustained, long-term measurements are needed in order to generate more reliable estimates of the seasonal cycles for the two stations.

### 3.1.4 $SF_6$

Figure 8 presents time series of $SF_6$ flask measurements and corresponding fitting curves at HLE, PON, and PBL. At HLE, the annual mean $SF_6$ mole fractions increased from $6.26 \pm 0.03$ to $7.38 \pm 0.01$ ppt between 2007 and 2011, which is in good agreement with the $SF_6$ trend observed at MLO during the same period (HLE: $0.29 \pm 0.05$ ppt yr$^{-1}$, $r^2 = 0.99$, $p < 0.001$; MLO: $0.29 \pm 0.03$ ppt yr$^{-1}$, $r^2 = 0.99$, $p < 0.001$; Figs. 8 and S9a, Table 1, Table S7). The annual mean $SF_6$ mole fractions at PON and PBL were lower than at HLE by $-0.060 \pm 0.030$ and $-0.002 \pm 0.097$ ppt, respectively. The slight negative gradient between PON, PBL and HLE is a reversed signal compared with the $SF_6$ observations at stations influenced by continental emissions in Europe and United States. For example, the $SF_6$ mole fractions at HUN over the years of 1997–2007 are higher than those at MLO and MHD by on average 0.33 and 0.19 ppt, respectively (Haszpra et al., 2008). We also analyzed the $SF_6$ gradients between two coastal European stations – BGU (41.97° N, 3.3° E, 30 m a.s.l.) and LPO (48.80° N, 3.57° W, 30 m a.s.l.) – and MHD, which are $0.10 \pm 0.03$ and $0.05 \pm 0.02$ ppt averaged over the period of 2007–2011, respectively. At HFM, the $SF_6$ mole fractions are higher than those of the NWR on average by $0.15 \pm 0.06$ ppt during 2007–2011 (Table S7). Given that the atmospheric lifetime of $SF_6$ is 800–3200 years (Ravishankara et al., 1993; Morris et al., 1995), the positive offsets between continental European and US stations and background reference stations suggest significant sources in Europe and the US. On the contrary, the slight negative offsets between PON, PBL and HLE imply weak $SF_6$ emissions over the Indian subcontinent, which is also indicated by recent high-frequency in-situ measurements at Darjeeling, India (27.03° N, 88.25° E, 2194 m a.s.l.), another station located in the eastern Himalayas (Ganesan et al., 2013). It is also worthwhile to note that high $SF_6$ values occur repeatedly at HLE and PBL in winter, which is likely re-





ACPD
15, 7171–7238, 2015



lated to episodic $SF_6$ pollution events from the Middle East and South/Southeast Asia, respectively (Figs. 8b and S6c).

The annual mean $SF_6$ seasonal cycles for HLE, PON, and PBL are presented in Fig. 9. The peak-to-peak amplitudes at the three stations are $0.15 \pm 0.03$, $0.24 \pm 0.02$, and $0.48 \pm 0.07$ ppt, respectively (Table 1). At HLE, the $SF_6$ seasonal cycle is bimodal as for $N_2O$, with an absolute maximum occurring in November (Student's $t$ test, $t = 2.425$, $p = 0.014$) and a secondary maximum in May (Student's $t$ test, $t = 2.443$, $p = 0.016$) (Table S8 for detailed $t$ test statistics). Given that $SF_6$ increases monotonously and that its sources are purely anthropogenic and not subject to seasonally variations (Maiss et al., 1996), the seasonal cycle of $SF_6$ should be driven by changes in atmospheric circulations, e.g., the SW monsoon convection and stratosphere-atmosphere exchange (Levin et al., 2002). We note that, at HLE, no enhancement of $SF_6$ during the SW monsoon season is recorded, unlike what is observed for $CH_4$ and $N_2O$ (Figs. 5 and 7). Although the CARIBIC aircraft flask measurements over the Indian region demonstrate an $SF_6$ enhancement in the upper troposphere at $\sim 30^\circ$ N (approximately where HLE is located) in August 2008, back-trajectories from the CARIBIC flights collected samples identified the influences of westerly jet transport, rather than the SW monsoon and sources from India (Schuck et al., 2010). The absence of $SF_6$ enhancement in summer at HLE confirms weak $SF_6$ emissions in India. At PBL, the $SF_6$ seasonal cycle is related to the monsoon circulation and convection (Figs. 9b and S6c). The maximum during November–December (Student's $t$ test, $t = 5.138$, $p < 0.001$; Table S8) is likely due to frequent episodic $SF_6$ polluted air masses transported southwesterly from Southeast Asia (Fig. S6c).

### 3.1.5 CO

The time series of CO flask measurements and corresponding smoothed curves are shown in Fig. 10. Over the period of 2007–2011, HLE recorded a slight decrease in CO mole fractions from $104.7 \pm 1.4$ to $99.4 \pm 2.2$ ppb, with an annual rate of $-2.2 \pm 0.0$ ppb yr$^{-1}$ ($r^2 = 0.65$, $p = 0.06$). CO at HLE is lower than at the two stations





ACPD
15, 7171–7238, 2015



further north in Asia, KZM and WLG (Novelli et al., 2014b), by on average 18.8 ± 2.5 and 30.2 ± 7.4 ppb, respectively (Table 1, Fig. 10c and d). The positive gradient between KZM, WLG and HLE does not only reflect decreasing CO with altitude and the N–S global gradient, but also suggests differences in regional emission sources. For example, compared to HLE, the CO signals at WLG are more influenced by transport of polluted air, especially during summer when about 30 % air masses pass over industrialized and urbanized areas southeast of the station (Zhang et al., 2011). Besides, the positive CO gradient between KZM, WLG and HLE may be further contributed by air masses of northern Siberia origin in summer (Fig. S4), with higher CO emissions from biomass burning and secondary CO from the oxidation of $CH_4$ and non-$CH_4$ hydrocarbons (Konovalov et al., 2014). At PON and PBL, the annual mean CO mole fractions are higher than that at HLE by on average 82.4 ± 10.7 and 52.5 ± 8.5 ppb, respectively (Table 1, Fig. 10a and b). The PON and PBL stations are influenced by CO regional emissions, mainly due to biofuel and agricultural burning over South and Southeast Asia (Lelieveld et al., 2001; Streets et al., 2003a, b; Yevich and Logan, 2003). We also note that, for all the five stations, CO time series show larger variability with respect to their corresponding smoothed curves than other species do (see the residual SD (RSD) in Table 1, Fig. 10), as a result of the unevenly distributed CO sources and short atmospheric lifetime (Novelli et al., 1992).

As shown in Fig. 11, the CO seasonal cycle at HLE reaches a maximum in mid-March and a minimum by the end of October, with a peak-to-peak amplitude of 28.4 ± 2.3 ppb (Table 1, Fig. 11). The phase of the mean CO seasonal cycle at HLE generally agrees with the ones observed at KZM and WLG, with a lag of up to 1 month in the timing of seasonal minimum at the two stations (Fig. 11c and d). In contrast with the three stations representative of large-scale free tropospheric air masses, the stations at the maritime boundary layer in the mid-to-high Northern Hemisphere observe the lowest CO values in July or August (Novelli et al., 1992, 1998), when the concentration of OH – the major sink of CO – is highest (Logan et al., 1981). The delay in timing of the seasonal CO minimum at the three free troposphere stations in Central and South





ACPD
15, 7171–7238, 2015



Asia compared to those boundary layer stations is due to the mixing time of regional surface CO emissions and the relatively short lifetime of CO (1–2 months on average). During summer, KZM and WLG sample air masses from Siberia impacted by CO fire emissions (Duncan et al., 2003; Kasischke et al., 2005), as well as CO-polluted air from urbanized and industrialized area (Zhang et al., 2011), while HLE is influenced by convective mixing of CO emissions from India, either from anthropogenic sources or oxidation of VOCs. It is interesting to note that the CO seasonal cycle at HLE does not show an enhancement during JAS as $CH_4$ and $N_2O$ do (Figs. 5 and 7), possibly as a result of OH oxidation that reduces CO and acts oppositely to vertical transport, and/or differences in seasonal emission patterns between CO and the other two species (Baker et al., 2012). However, CO enhancement during summer was observed in the upper troposphere over South Asia from the CARIBIC aircraft measurements at flight altitudes 8–12.5 km and Microwave Limb Sounder observations at 100–200 hPa (Li et al., 2005; Jiang et al., 2007a; Schuck et al., 2010). The differences in the CO seasonal cycles at different altitudes suggest faster transport (and younger air masses) at 10 km than at 5 km due to convection, controlling the vertical profile of CO, which makes it difficult to directly compare aircraft measurements in the upper troposphere and column remote sensing observations with surface data.

At PON and PBL, the mean CO seasonal cycles show maxima in the boreal winter and minima in the boreal summer, with peak-to-peak amplitudes of $78.2 \pm 11.6$ and $144.1 \pm 16.0$ ppb, respectively (Fig. 11a and b). A strong and positive correlation is found between detrended CO and $CH_4$ at PON ($r = 0.70$, $p < 0.001$) and PBL ($r = 0.84$, $p < 0.001$), suggesting that the seasonal cycles of both species are dominated by the seasonally varying atmospheric transport. During summer when the southwest monsoon prevails, surface CO at PON and PBL is low due to rapid convective uplifting and advection of clean air masses from the ocean. During winter, the two stations are influenced by northeasterly air masses enriched in CO from Northeast India and Southeast Asia (back-trajectories in Fig. S6d), influenced by biofuel and agricultural waste burning in these regions (Yevich and Logan, 2003; Lelieveld et al., 2001).





ACPD
15, 7171–7238, 2015



### 3.1.6 $H_2$

Figure 12 shows the time series of $H_2$ flask measurements with smoothed curves at HLE, PON, and PBL, respectively. No significant trend was observed at any of the three stations (Table 1, Fig. 12), consistent with the long-term $H_2$ measurements at other background stations during the last three decades (Novelli et al., 1999; Ehhalt and Rohrer, 2009; Grant et al., 2010). For the year 2008, comparing to KZM and WLG (Novelli et al., 2014a), HLE recorded higher $H_2$ mole fractions by ~ 40 ppb, reflecting the latitudinal gradient of $H_2$ with lower concentrations towards northern high latitudes, due to land uptake by soils (Novelli et al., 1999; Price et al., 2007; Hauglustaine and Ehhalt, 2002; Ehhalt and Rohrer, 2009). Note that these results based on only one-year comparison need to be confirmed by extended data more up-to-date, which are not available yet. At PON and PBL, the annual mean $H_2$ mole fractions were higher than at HLE by 29.8 ± 4.1 and 21.8 ± 4.6 ppb, respectively (Table 1; Fig. 12). Comparisons with $H_2$ measurements at Mariana Island, Guam (GMI – 13.39° N, 144.66° E, 0.00 m a.s.l.) (Novelli et al., 2014a), another maritime station in the western Pacific at a similar latitude as PON and PBL, also showed positive gradients of ~ 40 ppb (Fig. S10c and d; Table S9), suggesting substantial regional $H_2$ sources over the footprint area of PBL and PON. During October–March when the NE monsoon prevails, both PON and PBL receive $H_2$-enriched air masses from South and Southeast Asia, mainly influenced by fossil fuel combustion and biomass burning (Fig. S6e; GFED v3.1; Hauglustaine and Ehhalt, 2002; Price et al., 2007; Ehhalt and Rohrer, 2009; van der Werf et al., 2010). During April–September, with the northward movement of Intertropical Convergence Zone (ITCZ), the two stations are influenced by advection of air from south of the Equator. For PON, $H_2$-polluted air masses are occasionally sampled during JAS when the SW monsoon moves over the continent of South India with high population and heavy industry (Fig. S6e; Census India, 2011).

The mean $H_2$ seasonal cycle for HLE, PON, and PBL are presented in Fig. 13. At HLE, the peak-to-peak $H_2$ seasonal amplitude is 15.8 ± 2.2 ppb, less than half of the





ACPD
15, 7171–7238, 2015



seasonal amplitudes at BMW (39.6 ± 2.6 ppb) and MID (38.0 ± 2.4 ppb) of similar latitudes (Novelli et al., 2014a), and that at WLG (22.8 ± 3.0 ppb) (Figs. 13d and S11a, Tables 1 and S9). The maximum and minimum of $H_2$ occur in April and September, respectively. The dampening of the $H_2$ seasonal amplitude with increasing altitude was previously found for another high-altitude continental station at Jungfraujoch, Switzerland (JUN – 46.53° N, 7.98° E, 3580.00 m a.s.l.) (Bond et al., 2011), and was also captured by the GEOS-Chem global chemical transport model (Price et al., 2007). Since the soil sink dominates much of the surface $H_2$ seasonal cycle in the mid-to-high Northern Hemisphere (Hauglustaine and Ehhalt, 2002; Price et al., 2007; Bousquet et al., 2011; Yver et al., 2011; Yashiro et al., 2011), the smaller amplitude in the $H_2$ seasonal cycle at HLE can be explained mainly by the weakened soil sink with increasing altitude due to vertical mixing (Price et al., 2007; Bond et al., 2011).

At PON and PBL, the mean $H_2$ seasonal cycles are characterized by the peak-to-peak amplitudes of 21.6±3.4 and 21.3±5.0 ppb respectively, comparable to that at GMI (21.5±1.2 ppb) (Table 1, Table S9, Figs. 13a and b and S11b). At PBL, the $H_2$ maximum in March–April and a secondary increase during September–October coincide with the double biomass burning peaks in each hemisphere – in March for northern tropics, in August/September for southern tropics (van der Werf et al., 2006; Price et al., 2007; Bousquet et al., 2011; Yver et al., 2011). Given that the seasonal variation of soil $H_2$ uptake is probably small in the tropics (Price et al., 2007; Bousquet et al., 2011; Yver et al., 2011; Yashiro et al., 2011), this bimodal $H_2$ seasonal cycle at PBL can be driven by biomass burning. The April, and larger peak is likely due to $H_2$ emitted from biomass burning in South and Southeast Asia and transported by the NE monsoon, while the October peak is possibly a result of the long-range transport of $H_2$-polluted air from biomass burning in tropical Africa (Fig. S6e).

### 3.2 Synoptic variations

In this section we analyze synoptic variations of $CO_2$, $CH_4$, and CO by examining correlations between species, after subtracting the smoothed curve from the original





ACPD
15, 7171–7238, 2015



data. Ratios of trace gas mole fractions or their enhancements have been widely used in previous studies to partition contributions from different source types and origins (Langenfelds et al., 2002; Paris et al., 2008; Lopez et al., 2012), to estimate emissions of one species given emissions of another one that is better-known (Gamnitzer et al., 2006; Rivier et al., 2006; Turnbull et al., 2006; Schuck et al., 2010), and to provide valuable constraints on inversion of sources and sinks of trace gases (Xiao et al., 2004; Pison et al., 2009).

### 3.2.1 $\Delta CH_4/\Delta CO$

Figure 14 shows scatterplots of $CH_4$ and CO residuals with the orthogonal distance regression lines at HLE, PON, and PBL for different seasons. A significant and positive correlation between $CH_4$ and CO residuals (hereafter $\Delta CH_4/\Delta CO$, unit ppb ppb$^{-1}$) is found for all three stations throughout the year. Furthermore, the $\Delta CH_4/\Delta CO$ ratio also shows seasonal variation at each of the three stations. The most prominent feature is the occurrence of maximum slopes in July–September (also October–December at PON), especially at HLE and the generally higher ratios at this station. Wada et al. (2011) and Niwa et al. (2014) also reported increased summer $\Delta CH_4/\Delta CO$ over the western North Pacific, according to the in-situ measurements at several surface stations and aircraft flask measurements in the mid-troposphere. The main process for this seasonal variation of $\Delta CH_4/\Delta CO$ might be the enhanced emissions of biogenic $CH_4$ in summer (e.g., wetland and rice paddy emissions; Streets et al., 2003a; Yan et al., 2003) combined with concurrent lower anthropogenic CO emissions in summer than in winter (Streets et al., 2003a). The faster photochemical destruction of CO by increased OH during summer cannot explain such large changes (less than 15 % according to Wada et al., 2011).

At HLE, the $\Delta CH_4/\Delta CO$ ratio varies from $1.2 \pm 0.3$ to $4.0 \pm 1.2$ ppb ppb$^{-1}$ throughout the year, with a maximum in JAS, corresponding to the summer monsoon season (Fig. 14a–d). Based on the CARIBIC flights between 10 and 12 km from Frankfurt, Germany to Chennai, India, Baker et al. (2012) derived a $\Delta CH_4/\Delta CO$ ratio in the range





ACPD
15, 7171–7238, 2015



1.88(±0.22) to 4.43(±0.56) in JAS over South Asia. The maximum $\Delta CH_4/\Delta CO$ observed during summer in the mid-to-upper troposphere is the result of higher biogenic $CH_4$ emission over the Indian subcontinent, lower CO emissions, combined with frequent widespread convective uplift of surface air during the SW monsoon (Schuck et al., 2010; Baker et al., 2012). The CARIBIC flights recorded similar $\Delta CH_4/\Delta CO$ values to HLE, confirming that convection plays a dominant role compared to advection during the SW monsoon season. Outside the SW monsoon season, both the CARIBIC flights and HLE do generally not record strong effects of surface emissions due to the weakened vertical transport. With respect to the $\Delta CH_4/\Delta CO$ ratios for January–March, April–June and October–December, our estimates are 1.5 to 4 times of the ratios determined for air masses with signatures of fossil fuel combustion, according to several aircraft and ground observations in East and Southeast Asia (Table S10; Sawa et al., 2004; Lai et al., 2010; Wada et al., 2011; Niwa et al., 2014), which rules out fossil fuel combustion as an explanation for the higher ratios. Our ratios are comparable to $\Delta CH_4/\Delta CO$ values inferred for air masses of Siberian origin during winter (Table S10; Harris et al., 2000; Chi et al., 2013), and we also obtain similar estimates of $\Delta CH_4/\Delta CO$ from the flask measurements at KZM over the study period (the $\Delta CH_4/\Delta CO$ ratios for KZM are $0.8 \pm 0.2$, $1.7 \pm 0.2$ and $1.5 \pm 0.3$ ppb ppb$^{-1}$ for AMJ, OND and JFM, respectively), which are influenced by air masses originating from North Africa, the Middle East, and Central Asia as seen at HLE (see back-trajectories in Fig. S4). Given that oil and gas production accounts for 50–70 % of $CH_4$ emissions in these regions (EDGAR v4.2) and that over dry areas the daytime boundary layer is higher which favors injection of surface emissions into the troposphere, the preferential enrichment in $CH_4$ relative to CO at HLE may tentatively be attributed to fossil $CH_4$ emissions over gas extraction regions and transported eastwards by westerlies (Harris et al., 2000; Tohjima et al., 1996).

At PON and PBL, the $\Delta CH_4/\Delta CO$ ratios are in general considerably higher than 0.3 for all seasons, putting them in the range of ratios indicative of urban/industrial sources (Table S10; Harriss et al., 1994; Sawa et al., 2004; Xiao et al., 2004; Bak-





ACPD
15, 7171–7238, 2015



win et al., 1995; Lai et al., 2010; Wada et al., 2011; Niwa et al., 2014). However, this does not rule out contributions from biomass/biofuel burning with emissions having a typical $\Delta CH_4/\Delta CO$ ratio less than 0.3 (Mauzerall et al., 1998; Andreae and Merlet, 2001; Mühle et al., 2002). Considering that biofuel and agriculture waste burning are the primary energy source in rural India (Streets et al., 2003a; Yevich and Logan, 2003; Venkataraman et al., 2005), CO emissions from biofuel burning must be substantial (Lelieveld et al., 2001). This is the case for NE India located upwind of PON and PBL when the NE monsoon prevails during December–March. Nevertheless, the relatively low $\Delta CH_4/\Delta CO$ derived from biomass/biofuel burning could be increased by $CH_4$ emissions from livestock with similarly distributed sources (EDGAR v4.2). Emissions of both trace gases from livestock and biomass/biofuel burning in the Indian subcontinent compiled by EDGAR v4.2 also indicate a $CH_4$ to CO ratio of 0.64–0.69 over the period of 2000–2008, close to the atmospheric measurements of $\Delta CH_4/\Delta CO$ at PON and PBL during JFM (Fig. 14h and l).

### 3.2.2 $\Delta CH_4/\Delta CO_2$

The $\Delta CH_4/\Delta CO_2$ ratios are strongly influenced by the high variability of $CO_2$ and the interpretation is complex. Unlike the positive correlation between $CH_4$ and CO consistently observed at all three stations, the relationships between $CH_4$ and $CO_2$ residuals exhibit scattered and differences in the residual slopes for different stations and seasons (Fig. 15). At HLE, no significant correlations are found during AMJ, JAS, and OND (Fig. 15a–c), because $CH_4$ and $CO_2$ have distinct biogenic and/or photochemical sources and sinks over the mid-Northern latitudes. During JFM when biogenic $CO_2$ fluxes and anthropogenic emissions are positive to the atmosphere, there is a significant and positive relationship between $CH_4$ and $CO_2$, with a $\Delta CH_4/\Delta CO_2$ ratio of $45.6 \pm 1846.8\,\mathrm{ppb\,ppm^{-1}}$ ($r = 0.37$, $p = 0.03$; Fig. 15d). This value is close to the ratio of $CH_4$ and $CO_2$ anthropogenic emissions over North Africa (39.1–46.2 $\mathrm{mmol\,mol^{-1}}$), Central Asia (44.4–49.5 $\mathrm{mmol\,mol^{-1}}$) and to a lesser degree the Middle East (25.8–





ACPD
15, 7171–7238, 2015



28.4 mmol mol$^{-1}$) during the period of 2000–2010 (EDGAR v4.2), corresponding to the back-trajectories reaching HLE (Fig. 1). It should be noted that this estimate of $\Delta CH_4/\Delta CO_2$ is subject to large uncertainty according to the SD calculated with 1000 bootstrap replications (Fig. 15d), implying that $CH_4$ and $CO_2$ sources of various types and origins influence the HLE records.

At PON, in contrast to HLE, positive correlations occur between $CH_4$ and $CO_2$ residuals for all seasons except OND, with a $\Delta CH_4/\Delta CO_2$ ratio of $6.7 \pm 2.4$ ppb ppm$^{-1}$ ($r = 0.72$, $p < 0.001$) in AMJ and $8.5 \pm 0.9$ ppb ppm$^{-1}$ in JAS ($r = 0.74$, $p < 0.001$), respectively (Fig. 15e and f). The relatively narrow ranges of slopes compared to that for HLE and PBL likely suggest co-located local urban and industrial sources in South India upwind of PON during April–September (see back-trajectories in Fig. 1). Emissions from biofuel burning could be a common source for both $CH_4$ and $CO_2$, given the substantial biofuel use in South India (Yevich and Logan, 2003) and the biofuel burning emission ratio of $CH_4$ and $CO_2$ derived from previous studies (5–10 mmol mol$^{-1}$; Andreae and Merlet, 2001). Note that the CARIBIC flask measurements over India south of 20° N indicate a negative correlation between $CH_4$ and $CO_2$ at the altitudes of 10–12 km during July–September 2008 ($r = -0.80$, $p = 0.002$; Fig. S12a), interpreted as the concurrent strong uptake of $CO_2$ with enhanced emissions of $CH_4$ during the SW monsoon. During JFM when the NE monsoon predominates, $CH_4$ is positively correlated with $CO_2$ with a $\Delta CH_4/\Delta CO_2$ ratio of $31.9 \pm 1635.7$ ppb ppm$^{-1}$ ($r = 0.45$, $p = 0.02$; Fig. 15h). Like at HLE, this ratio is subject to large uncertainty due to variability in $CH_4$ and $CO_2$ sources. The ratio based on the CARIBIC observations in the upper troposphere (10–12 km) is $23.5 \pm 41.4$ ppb ppm$^{-1}$ ($r = 0.67$, $p = 0.004$; Fig. S12b). The inconsistency of the $\Delta CH_4/\Delta CO_2$ ratios estimated from the two datasets suggest that the flask measurements at the surface station PON do provide information more specific for constraining estimates of regional $CH_4$ and $CO_2$ fluxes.

Finally, at PBL, the prominent feature of the $CH_4$–$CO_2$ relationship is the significant and negative correlation observed during JAS, with a $\Delta CH_4/\Delta CO_2$ ratio of $-14.6 \pm 16.4$ ppb ppm$^{-1}$ ($r = -0.73$, $p = 0.007$; Fig. 15j). Since the time series of flask





ACPD
15, 7171–7238, 2015



measurements at PBL is relatively short and has large data gaps (Fig. S2), correlations between trace gases could be influenced by abnormal pollution events. For example, excluding the event with $CH_4$ residuals > +20 ppb (corresponding to the observation at PBL on 16 September 2009, the point marked with black circle in Fig. 15j) would substantially decrease the strength of negative correlation between $CH_4$ and $CO_2$ ($r = -0.54$, $p = 0.09$). We will investigate the $CH_4$ enriched event further in Sect. 3.3.

### 3.2.3 $\Delta CO/\Delta CO_2$

As shown in Fig. 16, at HLE, CO is positively correlated with $CO_2$ during AMJ, with a $\Delta CO/\Delta CO_2$ ratio of $35.8 \pm 12.1$ ppb ppm$^{-1}$ ($r = 0.53$, $p = 0.001$; Fig. 16a). During JFM, there is no significant relationship between CO and $CO_2$ ($r = 0.15$, $p = 0.39$; Fig. 16d). However, excluding an abnormal event with $\Delta CO_2 = -1.8$ ppm on 8 January 2007 (the point marked with black circle in Fig. 16d) would give a significant and positive correlation between CO and $CO_2$, with a $\Delta CO/\Delta CO_2$ ratio of $55.7 \pm 259.1$ ppb ppm$^{-1}$ ($r = 0.40$, $p = 0.02$; the red solid line in Fig. 16d). This ratio is less than half the emission ratio of CO to $CO_2$ from forest/grassland biomass burning (Mauzerall et al., 1998; Andreae and Merlet, 2001), but higher than ratios of anthropogenic combustion sources in developed countries that are typically in the range of 10–15 ppb ppm$^{-1}$ (e.g., Suntharalingam et al., 2004; Wada et al., 2011; Takegawa et al., 2004). This could be attributed not only to the lower combustion efficiency of fuels in North Africa, the Middle East, and Central Asia where air masses at HLE originate from, but also to additional contribution from biofuel burning with relatively high CO to $CO_2$ emission ratios (e.g., fuelwood, charcoal, agricultural residuals; Andreae and Merlet, 2001). Besides, the relatively high $\Delta CO/\Delta CO_2$ in JFM compared to AMJ may further indicate a contribution of CO emissions from residential biofuel burning in winter (Wada et al., 2011), especially in developing countries within the footprint area.

At PON, a positive and significant correlation between CO and $CO_2$ is found during AMJ, with a $\Delta CO/\Delta CO_2$ ratio of $13.4 \pm 76.8$ ppb ppm$^{-1}$ ($r = 0.46$, $p = 0.03$; Fig. 16e).





ACPD
15, 7171–7238, 2015



This ratio is similar to the ratios determined for air masses influenced by both fossil fuel emissions and biomass/biofuel burning during the same seasons. For example, based on the in-situ measurements in the upper troposphere during the CARIBIC flights between South China and Philippines in April 2007, Lai et al. (2010) reported the $\Delta CO/\Delta CO_2$ ratios of 15.6–29.3 ppb ppm$^{-1}$ during pollution events influenced by both biomass/biofuel burning and fossil fuel combustion in Indochinese Peninsula. At PBL, CO is significantly and negatively correlated with $CO_2$ during JAS ($r = -0.68$, $p = 0.01$; Fig. 16j). However, we note that the $CH_4$ abnormal event discussed in Sect. 3.2.2 is enriched in CO as well, and the negative relationship between CO and $CO_2$ would no longer exist if we removed the event ($r = -0.45$, $p = 0.16$). The simultaneous enhancement of CO and $CH_4$ may suggest possible influences of biomass burning episodes, which we will explore in detail in Sect. 3.3. During JFM, no significant relationship is found between CO and $CO_2$ for PON or PBL (Fig. 16h and l).

### 3.3 Elevated $CH_4$ and CO events at PBL

In this section, we discuss two elevated $CH_4$ and CO events at PBL during the SW monsoon season. Significant enhancements of $CH_4$ and CO were observed on September 16, 2009 (July 29, 2011), with residuals from smoothed curves as high as 34.2 (29.2) ppb and 36.2 (17.9) ppb for $CH_4$ and CO, respectively. To investigate the sources and origins that may have contributed to the two events, we analyzed $CH_4$ and CO measurements at Bukit Kototabang (BKT – 0.20° S, 100.32° E, 845.00 m a.s.l.), Indonesia, located upwind of PBL when the SW monsoon prevails. The flask measurements at BKT detected enhanced $CH_4$ and CO with a magnitude of 38.0 and 66.1 ppb on September 8, 2009, about one week before the occurrence of the first $CH_4$ and CO event at PBL (Fig. 17a). The in-situ measurements at BKT also showed $CH_4$ and CO enhancements about one week before the second event at PBL, lasting over the period of 17 July–21 July 2011 (Fig. 17b). The coincidence of the two abnormal $CH_4$ and CO events at PBL and BKT points to influences of polluted air masses with common sources and origins. Moreover, the fire radiative power (FRP, mW m$^{-2}$) during the





ACPD
15, 7171–7238, 2015



sampling dates implies that the two abnormal $CH_4$ and CO events may be related to fire emissions in Indonesia (GFAS product version 1.0; Kaiser et al., 2012; Fig. S13). A detailed analysis is needed in the future to further explore the linkage between atmospheric observations at the two stations during the SW monsoon season and the dominant sources of abnormal pollution events.

## 4 Conclusions

In this paper we present five-year (2007–2011) flask measurements of $CO_2$, $CH_4$, $N_2O$, $SF_6$, CO, and $H_2$ at three stations in India: Hanle (HLE), Pondicherry (PON) and Port-Blair (PBL). Of the three stations, HLE is located at high altitude and regarded as a continental background station in the mid-latitude of Northern Hemisphere; PON is a tropical surface station located on the southwest coast of India, while PBL is an oceanic station located on Andaman Islands, of similar latitude to PON. With a total of 188, 185, and 63 flask pairs sampled in India respectively at HLE, PON and PBL between 2007 and 2011, and analyzed at LSCE, the program represents an important logistical and analytical effort to produce a unique dataset of atmospheric trace gas observations over the Indian subcontinent. The observed records will serve as an important source of information to infer regional patterns of trace gas fluxes and atmospheric transport in this under-documented region. Several conclusions and implications are drawn from the first analyses of the datasets.

The offsets of the atmospheric mole fractions observed at PON and PBL, using HLE as a reference, suggest significant emission sources of $CO_2$, $CH_4$, $N_2O$, CO, and $H_2$ over the footprint of those stations, whereas $SF_6$ emission sources are weak. Particularly, the annual mean $N_2O$ mole fractions at PON and PBL are higher than at HLE by $3.1 \pm 0.3$ and $3.8 \pm 1.7$ ppb, notably larger than typical $N_2O$ gradients observed between stations in Europe or North America, indicating substantial $N_2O$ emissions. The analyses of the atmospheric mole fractions with back-trajectories at the three stations further confirmed emission sources from South and NE India, and SE Asia, all of which





ACPD
15, 7171–7238, 2015



are populous with high demand for food and energy, and thus high emissions from industrial, residential, and/or agricultural sectors.

The seasonal cycles for each trace gas reflect not only the seasonal variations of natural sources/sinks and anthropogenic emissions over the Indian subcontinent, but also the seasonally varying atmospheric transport, especially the monsoon circulations (including convection). The strong influence of monsoon circulations are well depicted by the contrasting phases of $CH_4$ seasonal cycles between HLE and PON/PBL. At HLE, the distinct $CH_4$ maximum during June–September can be attributed to the enhanced biogenic $CH_4$ emissions from wetlands and rice paddies in summer, combined with deep convection that is associated with the SW monsoon and mixes surface emissions into the mid-to-upper troposphere. By contrast, the $CH_4$ seasonal cycles at PON and PBL have seasonal minima during the SW monsoon season, reflecting influences of southern hemispheric air depleted in $CH_4$ transported at low altitude, as well as high rates of OH oxidation. Covariance between species variations at the synoptic scale further helps identification and attribution of different sources and sinks, like fossil fuel combustion, biofuel burning and biogenic emissions.

While the three stations have the potential to provide useful constraints on estimates of trace gas fluxes over South and NE India (for example, Swathi et al. (2013) reported a considerable reduction in the uncertainty by the inclusion of HLE in the $CO_2$ inversion over temperate Eurasia), the monitoring network will require further expansion to sample air masses from other parts of the Indian subcontinent. Recently a few other ground stations have been established to monitor GHGs and atmospheric pollutants along the western coast of India (Bhattacharya et al., 2009; Tiwari et al., 2011, 2014; Tiwari and Kumar, 2012) and in the Himalayas (Kumar et al., 2010; Ganesan et al., 2013). More efforts are needed to develop a comprehensive observation network with adequate spatial and temporal coverage in this region.

**The Supplement related to this article is available online at doi:10.5194/acpd-15-7171-2015-supplement.**





ACPD
15, 7171–7238, 2015



*Acknowledgements.* This study has been initiated within the framework of CaFICA-CEFIPRA project (2809-1). X. Lin acknowledges PhD funding support from AIRBUS D&S and ESF TTorch Short Visiting Grant for the 1st ICOS Science Conference (No. 6849). P. Ciais acknowledges support of the Synergy grant ERC-2013-SyG-610028 IMBALANCE-P of the European Research Council. The authors thank the engineers and staff from Indian Astronomical Observatory, Hanle, who have been helpful at the station in Hanle, and Manil Kumar, Shambhulinga and Prabhath Prabhu, who helped in flask sampling at Pondicherry University, B. Parmeshwar from National Institute of Ocean Technology for operating and maintaining the facilities in the stations. We also acknowledge the LSCE staff (L. Klenov, A. Crevier, B. Gal, C. Peureux, M. Grand, L. Hogrel, V. Bazantay and A. Orgun) taking in charge the RAMCES network logistics, measurements, and data processing.

## References

Attri, S. D. and Tyagi, A.: Climate Profile of India: Contribution to the Indian Network of Climate Change Assessment (NATIONAL COMMUNICATION-II) Minitry of Environment and Forests, Met Monograph No. Environment Meteorology-01/2010, India Meteorological Department, Ministry of Earth Sciences, New Delhi, 2010.

Andreae, M. O. and Merlet, P.: Emission of trace gases and aerosols from biomass burning, Global Biogeochem. Cy., 15, 955–966, doi:10.1029/2000gb001382, 2001.

Babu, S. S., Chaubey, J. P., Krishna Moorthy, K., Gogoi, M. M., Kompalli, S. K., Sreekanth, V., Bagare, S. P., Bhatt, B. C., Gaur, V. K., Prabhu, T. P., and Singh, N. S.: High altitude (4520 m a.m.s.l.) measurements of black carbon aerosols over western trans-Himalayas: seasonal heterogeneity and source apportionment, J. Geophys. Res.-Atmos., 116, D24201, doi:10.1029/2011jd016722, 2011.

Baker, A. K., Schuck, T. J., Brenninkmeijer, C. A. M., Rauthe-Schöch, A., Slemr, F., van Velthoven, P. F. J., and Lelieveld, J.: Estimating the contribution of monsoon-related biogenic production to methane emissions from South Asia using CARIBIC observations, Geophys. Res. Lett., 39, L10813, doi:10.1029/2012gl051756, 2012.

Bakwin, P. S., Tans, P. P., Zhao, C., Ussler, W., and Quesnell, E.: Measurements of carbon dioxide on a very tall tower, Tellus B, 47, 535–549, doi:10.1034/j.1600-0889.47.issue5.2.x, 1995.





ACPD
15, 7171–7238, 2015



Bakwin, P. S., Tans, P. P., Hurst, D. F., and Zhao, C.: Measurements of carbon dioxide on very tall towers: results of the NOAA/CMDL program, Tellus B, 50, 401–415, 1998.

Bange, H. W., Andreae, M. O., Lal, S., Law, C. S., Naqvi, S. W. A., Patra, P. K., Rixen, T., and Upstill-Goddard, R. C.: Nitrous oxide emissions from the Arabian Sea: A synthesis, Atmos. Chem. Phys., 1, 61–71, doi:10.5194/acp-1-61-2001, 2001.

Bhattacharya, S. K., Borole, D. V., Francey, R. J., Allison, C. E., Steele, L. P., Krummel, P. B., Langenfelds, R., Masarie, K. A., Tiwari, Y. K., and Patra, P. K.: Trace gases and $CO_2$ isotope records from Cabo de Rama, India, Curr. Sci. India, 97, 1336–1344, 2009.

Bond, S. W., Vollmer, M. K., Steinbacher, M., Henne, S., and Reimann, S.: Atmospheric molecular hydrogen ($H_2$): observations at the high-altitude site Jungfraujoch, Switzerland, Tellus B, 63, 64–76, doi:10.1111/j.1600-0889.2010.00509.x, 2011.

Bousquet, P., Yver, C., Pison, I., Li, Y. S., Fortems, A., Hauglustaine, D., Szopa, S., Rayner, P. J., Novelli, P., Langenfelds, R., Steele, P., Ramonet, M., Schmidt, M., Foster, P., Morfopoulos, C., and Ciais, P.: A three-dimensional synthesis inversion of the molecular hydrogen cycle: sources and sinks budget and implications for the soil uptake, J. Geophys. Res.-Atmos., 116, D01302, doi:10.1029/2010jd014599, 2011.

Chi, X., Winderlich, J., Mayer, J.-C., Panov, A. V., Heimann, M., Birmili, W., Heintzenberg, J., Cheng, Y., and Andreae, M. O.: Long-term measurements of aerosol and carbon monoxide at the ZOTTO tall tower to characterize polluted and pristine air in the Siberian taiga, Atmos. Chem. Phys., 13, 12271–12298, doi:10.5194/acp-13-12271-2013, 2013.

Dlugokencky, E. J., Myers, R. C., Lang, P. M., Masarie, K. A., Crotwell, A. M., Thoning, K. W., Hall, B. D., Elkins, J. W., and Steele, L. P.: Conversion of NOAA atmospheric dry air $CH_4$ mole fractions to a gravimetrically prepared standard scale, J. Geophys. Res.-Atmos., 110, D18306, doi:10.1029/2005jd006035, 2005.

Dlugokencky, E. J., Lang, P. M., Crotwell, A. M., Masarie, K. A., and Crotwell, M. J.: Atmospheric Methane Dry Air Mole Fractions from the NOAA ESRL Carbon Cycle Cooperative Global Air Sampling Network, 1983–2013, Version: 2014-06-24, available at: ftp://aftp.cmdl.noaa.gov/data/trace_gases/ch4/flask/surface/ (last access: 11 December 2014), 2014a.

Dlugokencky, E. J., Lang, P. M., Masarie, K. A., Crotwell, A. M., and Crotwell, M. J.: Atmospheric Carbon Dioxide Dry Air Mole Fractions from the NOAA ESRL Carbon Cycle Cooperative Global Air Sampling Network, 1968–2013, Version: 2014-06-27, available at: ftp://aftp.cmdl.noaa.gov/data/trace_gases/co2/flask/surface/ (last access: 11 December 2014), 2014b.





ACPD
15, 7171–7238, 2015



Draxler, R. R. and Rolph, G. D.: HYSPLIT (HYbrid Single-Particle Lagrangian Integrated Trajectory), Model access via NOAA ARL READY, available at: http://www.arl.noaa.gov/ready/hysplit4.html (last access: 9 January 2014), NOAA Air Resources Laboratory, Silver Spring, MD, 2003.

Duncan, B. N., Martin, R. V., Staudt, A. C., Yevich, R., and Logan, J. A.: Interannual and seasonal variability of biomass burning emissions constrained by satellite observations, J. Geophys. Res.-Atmos., 108, 4100, doi:10.1029/2002jd002378, 2003.

EC-JRC/PBL (European Commission, Joint Research Centre/Netherlands Environmental Assessment Agency): Emission Database for Global Atmospheric Research (EDGAR), release version 4.2: available at: http://edgar.jrc.ec.europa.eu (last access: 16 August 2014), 2011.

Ehhalt, D. H. and Rohrer, F.: The tropospheric cycle of $H_2$: a critical review, Tellus B, 61, 500–535, doi:10.1111/j.1600-0889.2009.00416.x, 2009.

Fang, S. X., Zhou, L. X., Tans, P. P., Ciais, P., Steinbacher, M., Xu, L., and Luan, T.: In situ measurement of atmospheric $CO_2$ at the four WMO/GAW stations in China, Atmos. Chem. Phys., 14, 2541–2554, doi:10.5194/acp-14-2541-2014, 2014.

Gadgil, S.: The Indian Monsoon and its variability, Annu. Rev. Earth Pl. Sc., 31, 429–467, doi:10.1146/annurev.earth.31.100901.141251, 2003.

Gamnitzer, U., Karstens, U., Kromer, B., Neubert, R. E. M., Meijer, H. A. J., Schroeder, H., and Levin, I.: Carbon monoxide: a quantitative tracer for fossil fuel $CO_2$?, J. Geophys. Res.-Atmos., 111, D22302, doi:10.1029/2005jd006966, 2006.

Ganesan, A. L., Chatterjee, A., Prinn, R. G., Harth, C. M., Salameh, P. K., Manning, A. J., Hall, B. D., Mühle, J., Meredith, L. K., Weiss, R. F., O'Doherty, S., and Young, D.: The variability of methane, nitrous oxide and sulfur hexafluoride in Northeast India, Atmos. Chem. Phys., 13, 10633–10644, doi:10.5194/acp-13-10633-2013, 2013.

Garg, A., Shukla, P. R., Kapshe, M., and Menon, D.: Indian methane and nitrous oxide emissions and mitigation flexibility, Atmos. Environ., 38, 1965–1977, doi:10.1016/j.atmosenv.2003.12.032, 2004.

Garg, A., Shukla, P. R., and Upadhyay, J.: $N_2O$ emissions of India: an assessment of temporal, regional and sector trends, Climatic Change, 110, 755–782, doi:10.1007/s10584-011-0094-9, 2012.

Goswami, B. N.: South Asian Monsoon, in: Intraseasonal Variability in the Atmospheric Ocean Climate System, edited by: Lau, W. K. M. and Waliser, D. E., Springer and Praxis Publishing, Chichester, UK, 2005.





ACPD
15, 7171–7238, 2015



Grant, A., Witham, C. S., Simmonds, P. G., Manning, A. J., and O'Doherty, S.: A 15 year record of high-frequency, in situ measurements of hydrogen at Mace Head, Ireland, Atmos. Chem. Phys., 10, 1203–1214, doi:10.5194/acp-10-1203-2010, 2010.

Hall, B. D., Dutton, G. S., and Elkins, J. W.: The NOAA nitrous oxide standard scale for atmospheric observations, J. Geophys. Res.-Atmos., 112, D09305, doi:10.1029/2006jd007954, 2007.

Harris, J. M., Dlugokencky, E. J., Oltmans, S. J., Tans, P. P., Conway, T. J., Novelli, P. C., Thoning, K. W., and Kahl, J. D. W.: An interpretation of trace gas correlations during Barrow, Alaska, winter dark periods, 1986–1997, J. Geophys. Res.-Atmos., 105, 17267–17278, doi:10.1029/2000jd900167, 2000.

Harriss, R. C., Sachse, G. W., Collins, J. E., Wade, L., Bartlett, K. B., Talbot, R. W., Browell, E. V., Barrie, L. A., Hill, G. F., and Burney, L. G.: Carbon monoxide and methane over Canada: July–August 1990, J. Geophys. Res.-Atmos., 99, 1659–1669, doi:10.1029/93jd01906, 1994.

Haszpra, L., Barcza, Z., Hidy, D., Szilágyi, I., Dlugokencky, E., and Tans, P.: Trends and temporal variations of major greenhouse gases at a rural site in Central Europe, Atmos. Environ., 42, 8707–8716, doi:10.1016/j.atmosenv.2008.09.012, 2008.

Hauglustaine, D. A. and Ehhalt, D. H.: A three-dimensional model of molecular hydrogen in the troposphere, J. Geophys. Res.-Atmos., 107, 4330, doi:10.1029/2001jd001156, 2002.

Hauglustaine, D. A., Hourdin, F., Jourdain, L., Filiberti, M. A., Walters, S., Lamarque, J. F., and Holland, E. A.: Interactive chemistry in the Laboratoire de Météorologie Dynamique general circulation model: description and background tropospheric chemistry evaluation, J. Geophys. Res.-Atmos., 109, D04314, doi:10.1029/2003jd003957, 2004.

IPCC: Climate Change 2013: The Physical Science Basis. Contribution of Working Group I to the Fifth Assessment Report of the Intergovernmental Panel on Climate Change, Cambridge University Press, Cambridge, 2013.

IPCC: Climate Change 2014: Impacts, Adaptation, and Vulnerability. Part A: Global and Sectoral Aspects. Contribution of Working Group II to the Fifth Assessment Report of the Intergovernmental Panel on Climate Change, edited by: Field, C. B., Barros, V. R., Dokken, D. J., Mach, K. J., Mastrandrea, M. D., Bilir, T. E., Chatterjee, M., Ebi, K. L., Estrada, Y. O., Genova, R. C., Girma, B., Kissel, E. S., Levy, A. N., MacCracken, S., Mastrandrea, P. R., and White, L. L., Cambridge University Press, Cambridge, UK and New York, NY, USA, 2014a.

IPCC: Climate Change 2014: Impacts, Adaptation, and Vulnerability. Part B: Regional Aspects. Contribution of Working Group II to the Fifth Assessment Report of the Intergovernmental





ACPD
15, 7171–7238, 2015



Panel on Climate Change, edited by: Barros, V. R., Field, C. B., Dokken, D. J., Mastrandrea, M. D., Mach, K. J., Bilir, T. E., Chatterjee, M., Ebi, K. L., Estrada, Y. O., Genova, R. C., Girma, B., Kissel, E. S., Levy, A. N., MacCracken, S., Mastrandrea, P. R., and White, L. L., Cambridge University Press, Cambridge, UK and New York, NY, USA, 2014b.

Jiang, J. H., Livesey, N. J., Su, H., Neary, L., McConnell, J. C., and Richards, N. A. D.: Connecting surface emissions, convective uplifting, and long-range transport of carbon monoxide in the upper troposphere: new observations from the Aura Microwave Limb Sounder, Geophys. Res. Lett., 34, L18812, doi:10.1029/2007gl030638, 2007a.

Jiang, X., Ku, W. L., Shia, R.-L., Li, Q., Elkins, J. W., Prinn, R. G., and Yung, Y. L.: Seasonal cycle of $N_2O$: analysis of data, Global Biogeochem. Cy., 21, GB1006, doi:10.1029/2006gb002691, 2007b.

Jordan, A. and Steinberg, B.: Calibration of atmospheric hydrogen measurements, Atmos. Meas. Tech., 4, 509–521, doi:10.5194/amt-4-509-2011, 2011.

Kaiser, J. W., Heil, A., Andreae, M. O., Benedetti, A., Chubarova, N., Jones, L., Morcrette, J.-J., Razinger, M., Schultz, M. G., Suttie, M., and van der Werf, G. R.: Biomass burning emissions estimated with a global fire assimilation system based on observed fire radiative power, Biogeosciences, 9, 527–554, doi:10.5194/bg-9-527-2012, 2012.

Kasischke, E. S., Hyer, E. J., Novelli, P. C., Bruhwiler, L. P., French, N. H. F., Sukhinin, A. I., Hewson, J. H., and Stocks, B. J.: Influences of boreal fire emissions on Northern Hemisphere atmospheric carbon and carbon monoxide, Global Biogeochem. Cy., 19, GB1012, doi:10.1029/2004gb002300, 2005.

Konovalov, I. B., Berezin, E. V., Ciais, P., Broquet, G., Beekmann, M., Hadji-Lazaro, J., Clerbaux, C., Andreae, M. O., Kaiser, J. W., and Schulze, E.-D.: Constraining $CO_2$ emissions from open biomass burning by satellite observations of co-emitted species: a method and its application to wildfires in Siberia, Atmos. Chem. Phys., 14, 10383–10410, doi:10.5194/acp-14-10383-2014, 2014.

Kumar, R., Naja, M., Venkataramani, S., and Wild, O.: Variations in surface ozone at Nainital: a high-altitude site in the central Himalayas, J. Geophys. Res.-Atmos., 115, D16302, doi:10.1029/2009jd013715, 2010.

Kurokawa, J., Ohara, T., Morikawa, T., Hanayama, S., Janssens-Maenhout, G., Fukui, T., Kawashima, K., and Akimoto, H.: Emissions of air pollutants and greenhouse gases over Asian regions during 2000–2008: Regional Emission inventory in ASia (REAS) version 2, Atmos. Chem. Phys., 13, 11019–11058, doi:10.5194/acp-13-11019-2013, 2013.





ACPD
15, 7171–7238, 2015



Lai, S. C., Baker, A. K., Schuck, T. J., van Velthoven, P., Oram, D. E., Zahn, A., Hermann, M., Weigelt, A., Slemr, F., Brenninkmeijer, C. A. M., and Ziereis, H.: Pollution events observed during CARIBIC flights in the upper troposphere between South China and the Philippines, Atmos. Chem. Phys., 10, 1649–1660, doi:10.5194/acp-10-1649-2010, 2010.

Langenfelds, R. L., Francey, R. J., Pak, B. C., Steele, L. P., Lloyd, J., Trudinger, C. M., and Allison, C. E.: Interannual growth rate variations of atmospheric $CO_2$ and its $\delta^{13}C$, $H_2$, $CH_4$, and CO between 1992 and 1999 linked to biomass burning, Global Biogeochem. Cy., 16, 1048, doi:10.1029/2001gb001466, 2002.

Lawrence, M. G. and Lelieveld, J.: Atmospheric pollutant outflow from southern Asia: a review, Atmos. Chem. Phys., 10, 11017–11096, doi:10.5194/acp-10-11017-2010, 2010.

Lelieveld, J., Crutzen, P. J., Ramanathan, V., Andreae, M. O., Brenninkmeijer, C. A. M., Campos, T., Cass, G. R., Dickerson, R. R., Fischer, H., de Gouw, J. A., Hansel, A., Jefferson, A., Kley, D., de Laat, A. T. J., Lal, S., Lawrence, M. G., Lobert, J. M., Mayol-Bracero, O. L., Mitra, A. P., Novakov, T., Oltmans, S. J., Prather, K. A., Reiner, T., Rodhe, H., Scheeren, H. A., Sikka, D., and Williams, J.: The Indian Ocean Experiment: widespread air pollution from South and Southeast Asia, Science, 291, 1031–1036, 2001.

Le Quéré, C., Moriarty, R., Andrew, R. M., Peters, G. P., Ciais, P., Friedlingstein, P., Jones, S. D., Sitch, S., Tans, P., Arneth, A., Boden, T. A., Bopp, L., Bozec, Y., Canadell, J. G., Chevallier, F., Cosca, C. E., Harris, I., Hoppema, M., Houghton, R. A., House, J. I., Jain, A., Johannessen, T., Kato, E., Keeling, R. F., Kitidis, V., Klein Goldewijk, K., Koven, C., Landa, C. S., Landschützer, P., Lenton, A., Lima, I. D., Marland, G., Mathis, J. T., Metzl, N., Nojiri, Y., Olsen, A., Ono, T., Peters, W., Pfeil, B., Poulter, B., Raupach, M. R., Regnier, P., Rödenbeck, C., Saito, S., Salisbury, J. E., Schuster, U., Schwinger, J., Séférian, R., Segschneider, J., Steinhoff, T., Stocker, B. D., Sutton, A. J., Takahashi, T., Tilbrook, B., van der Werf, G. R., Viovy, N., Wang, Y.-P., Wanninkhof, R., Wiltshire, A., and Zeng, N.: Global carbon budget 2014, Earth Syst. Sci. Data Discuss., 7, 521–610, doi:10.5194/essdd-7-521-2014, 2014.

Levin, I., Ciais, P., Langenfelds, R., Schmidt, M., Ramonet, M., Sidorov, K., Tchebakova, N., Gloor, M., Heimann, M., Schulze, E. D., Vygodskaya, N. N., Shibistova, O., and Lloyd, J.: Three years of trace gas observations over the EuroSiberian domain derived from aircraft sampling – a concerted action, Tellus B, 54, 696–712, doi:10.1034/j.1600-0889.2002.01352.x, 2002.





ACPD
15, 7171–7238, 2015



Li, Q., Jiang, J. H., Wu, D. L., Read, W. G., Livesey, N. J., Waters, J. W., Zhang, Y., Wang, B., Filipiak, M. J., Davis, C. P., Turquety, S., Wu, S., Park, R. J., Yantosca, R. M., and Jacob, D. J.: Convective outflow of South Asian pollution: a global CTM simulation compared with EOS MLS observations, Geophys. Res. Lett., 32, L14826, doi:10.1029/2005gl022762, 2005.

Liao, T., Camp, C. D., and Yung, Y. L.: The seasonal cycle of $N_2O$, Geophys. Res. Lett., 31, L17108, doi:10.1029/2004gl020345, 2004.

Logan, J. A., Prather, M. J., Wofsy, S. C., and McElroy, M. B.: Tropospheric chemistry: a global perspective, J. Geophys. Res.-Oceans, 86, 7210–7254, doi:10.1029/JC086iC08p07210, 1981.

Lopez, M.: Estimation des émissions de gaz à effet de serre à différentes échelles en France à l'aide d'observations de haute précision, Ph.D. thesis, Université Paris-Sud, Paris, 2012.

Lopez, M., Schmidt, M., Ramonet, M., Bonne, J.-L., Colomb, A., Kazan, V., Laj, P., and Pichon, J.-M.: A gas chromatograph system for semi-continuous greenhouse gas measurements at Puy-de-Dôme station, Center France, submitted, 2014.

Machida, T., Matsueda, H., Sawa, Y., Nakagawa, Y., Hirotani, K., Kondo, N., Goto, K., Nakazawa, T., Ishikawa, K., and Ogawa, T.: Worldwide measurements of atmospheric $CO_2$ and other trace gas species using commercial airlines, J. Atmos. Ocean. Tech., 25, 1744–1754, doi:10.1175/2008jtecha1082.1, 2008.

Maiss, M., Steele, L. P., Francey, R. J., Fraser, P. J., Langenfelds, R. L., Trivett, N. B. A., and Levin, I.: Sulfur hexafluoride – a powerful new atmospheric tracer, Atmos. Environ., 30, 1621–1629, doi:10.1016/1352-2310(95)00425-4, 1996.

Mauzerall, D. L., Logan, J. A., Jacob, D. J., Anderson, B. E., Blake, D. R., Bradshaw, J. D., Heikes, B., Sachse, G. W., Singh, H., and Talbot, B.: Photochemistry in biomass burning plumes and implications for tropospheric ozone over the tropical South Atlantic, J. Geophys. Res.-Atmos., 103, 8401–8423, doi:10.1029/97jd02612, 1998.

Messager, C.: Estimation des flux de gaz à effet de serre à l'échelle régionale à partir de mesures atmosphériques, Université Paris 7 – Denis Diderot, Paris, 2007.

Minschwaner, K., Salawitch, R. J., and McElroy, M. B.: Absorption of solar radiation by $O_2$: implications for $O_3$ and lifetimes of $N_2O$, $CFCl_3$, and $CF_2Cl_2$, J. Geophys. Res.-Atmos., 98, 10543–10561, doi:10.1029/93jd00223, 1993.

Montzka, S. A., Dlugokencky, E. J., and Butler, J. H.: Non-$CO_2$ greenhouse gases and climate change, Nature, 476, 43–50, 2011.





ACPD
15, 7171–7238, 2015



Moorthy, K. K., Sreekanth, V., Chaubey, J. P., Gogoi, M. M., Babu, S. S., Kompalli, S. K., Bagare, S. P., Bhatt, B. C., Gaur, V. K., Prabhu, T. P., and Singh, N. S.: Fine and ultrafine particles at near-free tropospheric environment over the high-altitude station Hanle in the Trans-Himalaya: new particle formation and size distribution, J. Geophys. Res.-Atmos., 116, D20212, doi:10.1029/2011JD016343, 2011.

Morgan, C. G., Allen, M., Liang, M. C., Shia, R. L., Blake, G. A., and Yung, Y. L.: Isotopic fractionation of nitrous oxide in the stratosphere: comparison between model and observations, J. Geophys. Res.-Atmos., 109, D04305, doi:10.1029/2003jd003402, 2004.

Morris, R. A., Miller, T. M., Viggiano, A. A., Paulson, J. F., Solomon, S., and Reid, G.: Effects of electron and ion reactions on atmospheric lifetimes of fully fluorinated compounds, J. Geophys. Res.-Atmos., 100, 1287–1294, doi:10.1029/94jd02399, 1995.

Mühle, J., Brenninkmeijer, C. A. M., Rhee, T. S., Slemr, F., Oram, D. E., Penkett, S. A., and Zahn, A.: Biomass burning and fossil fuel signatures in the upper troposphere observed during a CARIBIC flight from Namibia to Germany, Geophys. Res. Lett., 29, 1910, doi:10.1029/2002gl015764, 2002.

Niwa, Y., Machida, T., Sawa, Y., Matsueda, H., Schuck, T. J., Brenninkmeijer, C. A. M., Imasu, R., and Satoh, M.: Imposing strong constraints on tropical terrestrial $CO_2$ fluxes using passenger aircraft based measurements, J. Geophys. Res.-Atmos., 117, D11303, doi:10.1029/2012jd017474, 2012.

Niwa, Y., Tsuboi, K., Matsueda, H., Sawa, Y., Machida, T., Nakamura, M., Kawasato, T., Saito, K., Takatsuji, S., Tsuji, K., Nishi, H., Dehara, K., Baba, Y., Kuboike, D., Iwatsubo, S., Ohmori, H., and Hanamiya, Y.: Seasonal variations of $CO_2$, $CH_4$, $N_2O$ and CO in the mid-troposphere over the Western North Pacific observed using a C-130H cargo aircraft, J. Meteorol. Soc. Jpn., 92, 55–70, doi:10.2151/jmsj.2014-104, 2014.

Novelli, P. C., Steele, L. P., and Tans, P. P.: Mixing ratios of carbon monoxide in the troposphere, J. Geophys. Res.-Atmos., 97, 20731–20750, doi:10.1029/92jd02010, 1992.

Novelli, P. C., Masarie, K. A., and Lang, P. M.: Distributions and recent changes of carbon monoxide in the lower troposphere, J. Geophys. Res.-Atmos., 103, 19015–19033, doi:10.1029/98jd01366, 1998.

Novelli, P. C., Lang, P. M., Masarie, K. A., Hurst, D. F., Myers, R., and Elkins, J. W.: Molecular hydrogen in the troposphere: global distribution and budget, J. Geophys. Res.-Atmos., 104, 30427–30444, doi:10.1029/1999jd900788, 1999.





ACPD
15, 7171–7238, 2015



Novelli, P. C., Lang, P. M., and Masarie, K. A.: Atmospheric Hydrogen Dry Air Mole Fractions from the NOAA ESRL Carbon Cycle Cooperative Global Air Sampling Network, 1988–2009, Version: 2014-08-27, available at: ftp://aftp.cmdl.noaa.gov/data/trace_gases/h2/flask/surface/ (last access: 11 December 2014), 2014a.

Novelli, P. C. and Masarie, K. A.: Atmospheric Carbon Monoxide Dry Air Mole Fractions from the NOAA ESRL Carbon Cycle Cooperative Global Air Sampling Network, 1988–2013, Version: 2014-07-02, available at: ftp://aftp.cmdl.noaa.gov/data/trace_gases/co/flask/surface/ (last access: 11 December 2014), 2014b.

Paris, J. D., Ciais, P., Nédélec, P., Ramonet, M., Belan, B. D., Arshinov, M. Y., Golitsyn, G. S., Granberg, I., Stohl, A., Cayez, G., Athier, G., Boumard, F., and Cousin, J. M.: The YAK-AEROSIB transcontinental aircraft campaigns: new insights on the transport of $CO_2$, CO and $O_3$ across Siberia, Tellus B, 60, 551–568, doi:10.1111/j.1600-0889.2008.00369.x, 2008.

Park, M., Randel, W. J., Gettelman, A., Massie, S. T., and Jiang, J. H.: Transport above the Asian summer monsoon anticyclone inferred from Aura Microwave Limb Sounder tracers, J. Geophys. Res.-Atmos., 112, D16309, doi:10.1029/2006jd008294, 2007.

Pathak, H., Bhatia, A., Jain, N., and Aggarwal, P. K.: Greenhouse gas emission and mitigation in Indian agriculture – a review, in: ING Bulletins on Regional Assessment of Reactive Nitrogen, Bulletin No. 19, edited by: Singh, B., SCON-ING, New Delhi, I–IV and 1–34, 2010.

Patra, P., Takigawa, M., Ishijima, K., Choi, B.-C., Cunnold, D., J. Dlugokencky, E., Fraser, P., J. Gomez-Pelaez, A., Goo, T.-Y., Kim, J.-S., Krummel, P., Langenfelds, R., Meinhardt, F., Mukai, H., O'Doherty, S., Prinn, R. G., Simmonds, P., Steele, P., Tohjima, Y., Tsuboi, K., Uhse, K., Weiss, R., Worthy, D., and Nakazawa, T.: Growth rate, seasonal, synoptic, diurnal variations and budget of methane in the lower atmosphere, J. Meteorol. Soc. Jpn., 87, 635–663, 2009.

Patra, P. K., Lal, S., Venkataramani, S., de Sousa, S. N., Sarma, V. V. S. S., and Sardesai, S.: Seasonal and spatial variability in $N_2O$ distribution in the Arabian Sea, Deep-Sea Res. Pt. I, 46, 529–543, doi:10.1016/S0967-0637(98)00071-5, 1999.

Patra, P. K., Houweling, S., Krol, M., Bousquet, P., Belikov, D., Bergmann, D., Bian, H., Cameron-Smith, P., Chipperfield, M. P., Corbin, K., Fortems-Cheiney, A., Fraser, A., Gloor, E., Hess, P., Ito, A., Kawa, S. R., Law, R. M., Loh, Z., Maksyutov, S., Meng, L., Palmer, P. I., Prinn, R. G., Rigby, M., Saito, R., and Wilson, C.: TransCom model simulations of $CH_4$ and related species: linking transport, surface flux and chemical loss with $CH_4$ variability in the tro-





ACPD
15, 7171–7238, 2015



posphere and lower stratosphere, Atmos. Chem. Phys., 11, 12813–12837, doi:10.5194/acp-11-12813-2011, 2011a.
Patra, P. K., Niwa, Y., Schuck, T. J., Brenninkmeijer, C. A. M., Machida, T., Matsueda, H., and Sawa, Y.: Carbon balance of South Asia constrained by passenger aircraft $CO_2$ measurements, Atmos. Chem. Phys., 11, 4163–4175, doi:10.5194/acp-11-4163-2011, 2011b.
Patra, P. K., Canadell, J. G., Houghton, R. A., Piao, S. L., Oh, N.-H., Ciais, P., Manjunath, K. R., Chhabra, A., Wang, T., Bhattacharya, T., Bousquet, P., Hartman, J., Ito, A., Mayorga, E., Niwa, Y., Raymond, P. A., Sarma, V. V. S. S., and Lasco, R.: The carbon budget of South Asia, Biogeosciences, 10, 513–527, doi:10.5194/bg-10-513-2013, 2013.
Peylin, P., Law, R. M., Gurney, K. R., Chevallier, F., Jacobson, A. R., Maki, T., Niwa, Y., Patra, P. K., Peters, W., Rayner, P. J., Rödenbeck, C., van der Laan-Luijkx, I. T., and Zhang, X.: Global atmospheric carbon budget: results from an ensemble of atmospheric $CO_2$ inversions, Biogeosciences, 10, 6699–6720, doi:10.5194/bg-10-6699-2013, 2013.
Pison, I., Bousquet, P., Chevallier, F., Szopa, S., and Hauglustaine, D.: Multi-species inversion of $CH_4$, CO and $H_2$ emissions from surface measurements, Atmos. Chem. Phys., 9, 5281–5297, doi:10.5194/acp-9-5281-2009, 2009.
Price, H., Jaeglé, L., Rice, A., Quay, P., Novelli, P. C., and Gammon, R.: Global budget of molecular hydrogen and its deuterium content: constraints from ground station, cruise, and aircraft observations, J. Geophys. Res.-Atmos., 112, D22108, doi:10.1029/2006jd008152, 2007.
Ramonet, M., Ciais, P., Nepomniachii, I., Sidorov, K., Neubert, R. E. M., Langendörfer, U., Picard, D., Kazan, V., Biraud, S., Gusti, M., Kolle, O., Schulze, E. D., and Lloyd, J.: Three years of aircraft-based trace gas measurements over the Fyodorovskoye southern taiga forest, 300 km north-west of Moscow, Tellus B, 54, 713–734, doi:10.1034/j.1600-0889.2002.01358.x, 2002.
Ramonet, M., Indira, N. K., Bhatt, B. C., Delmotte, M., Schmidt, M., Wastine, B., Vuillemin, C., Gal, B., Lin, X., Paris, J. D., Cloué, O., Stohl, A., Conway, T. J., Ciais, P., Swathi, P. S., and Gaur, V. K.: Atmospheric $CO_2$ monitoring at Hanle, India, in preparation, 2015.
Ravishankara, A. R., Solomon, S., Turnipseed, A. A., and Warren, R. F.: Atmospheric lifetimes of long-lived halogenated species, Science, 259, 194–199, 1993.
Rayner, P. J., Law, R. M., Allison, C. E., Francey, R. J., Trudinger, C. M., and Pickett-Heaps, C.: Interannual variability of the global carbon cycle (1992–2005) inferred by inver-





ACPD
15, 7171–7238, 2015



sion of atmospheric $CO_2$ and $\delta^{13}CO_2$ measurements, Global Biogeochem. Cy., 22, GB3008, doi:10.1029/2007gb003068, 2008.
Rivier, L., Ciais, P., Hauglustaine, D. A., Bakwin, P., Bousquet, P., Peylin, P., and Klonecki, A.: Evaluation of $SF_6$, $C_2Cl_4$, and CO to approximate fossil fuel $CO_2$ in the Northern Hemisphere using a chemistry transport model, J. Geophys. Res.-Atmos., 111, D16311, doi:10.1029/2005jd006725, 2006.
Saikawa, E., Prinn, R. G., Dlugokencky, E., Ishijima, K., Dutton, G. S., Hall, B. D., Langenfelds, R., Tohjima, Y., Machida, T., Manizza, M., Rigby, M., O'Doherty, S., Patra, P. K., Harth, C. M., Weiss, R. F., Krummel, P. B., van der Schoot, M., Fraser, P. J., Steele, L. P., Aoki, S., Nakazawa, T., and Elkins, J. W.: Global and regional emissions estimates for $N_2O$, Atmos. Chem. Phys., 14, 4617–4641, doi:10.5194/acp-14-4617-2014, 2014.
Sawa, Y., Matsueda, H., Makino, Y., Inoue, H. Y., Murayama, S., Hirota, M., Tsutsumi, Y., Zaizen, Y., Ikegami, M., and Okada, K.: Aircraft Observation of $CO_2$, CO, $O_3$ and $H_2$ over the North Pacific during the PACE-7 Campaign, Tellus B, 56, 2–20, doi:10.1111/j.1600-0889.2004.00088.x, 2004.
Schuck, T. J., Brenninkmeijer, C. A. M., Baker, A. K., Slemr, F., von Velthoven, P. F. J., and Zahn, A.: Greenhouse gas relationships in the Indian summer monsoon plume measured by the CARIBIC passenger aircraft, Atmos. Chem. Phys., 10, 3965–3984, doi:10.5194/acp-10-3965-2010, 2010.
Schuck, T. J., Ishijima, K., Patra, P. K., Baker, A. K., Machida, T., Matsueda, H., Sawa, Y., Umezawa, T., Brenninkmeijer, C. A. M., and Lelieveld, J.: Distribution of methane in the tropical upper troposphere measured by CARIBIC and CONTRAIL aircraft, J. Geophys. Res.-Atmos., 117, D19304, doi:10.1029/2012jd018199, 2012.
Sivakumar, I. and Anitha, M.: Education and girl children in Puducherry region: problems and perspective, Int. J. Soc. Sci. Interdiscipl. Res., 1, 175–184, 2012.
Streets, D. G., Bond, T. C., Carmichael, G. R., Fernandes, S. D., Fu, Q., He, D., Klimont, Z., Nelson, S. M., Tsai, N. Y., Wang, M. Q., Woo, J. H., and Yarber, K. F.: An inventory of gaseous and primary aerosol emissions in Asia in the year 2000, J. Geophys. Res.-Atmos., 108, 8809, doi:10.1029/2002jd003093, 2003a.
Streets, D. G., Yarber, K. F., Woo, J. H., and Carmichael, G. R.: Biomass burning in Asia: annual and seasonal estimates and atmospheric emissions, Global Biogeochem. Cy., 17, 1099, doi:10.1029/2003gb002040, 2003b.





ACPD
15, 7171–7238, 2015



Suntharalingam, P., Jacob, D. J., Palmer, P. I., Logan, J. A., Yantosca, R. M., Xiao, Y., Evans, M. J., Streets, D. G., Vay, S. L., and Sachse, G. W.: Improved quantification of Chinese carbon fluxes using $CO_2$/CO correlations in Asian outflow, J. Geophys. Res.-Atmos., 109, D18S18, doi:10.1029/2003jd004362, 2004.

Swathi, P. S., Indira, N. K., Rayner, P. J., Ramonet, M., Jagadheesha, D., Bhatt, B. C., Gaur, V. K.: Robust inversion of carbon dioxide fluxes over temperate Eurasia in 2006–2008, Curr. Sci. India, 105, 201–208, 2013.

Takegawa, N., Kondo, Y., Koike, M., Chen, G., Machida, T., Watai, T., Blake, D. R., Streets, D. G., Woo, J. H., Carmichael, G. R., Kita, K., Miyazaki, Y., Shirai, T., Liley, J. B., and Ogawa, T.: Removal of $NO_x$ and $NO_y$ in Asian outflow plumes: aircraft measurements over the western Pacific in January 2002, J. Geophys. Res.-Atmos., 109, D23S04, doi:10.1029/2004jd004866, 2004.

Thompson, R. L., Chevallier, F., Crotwell, A. M., Dutton, G., Langenfelds, R. L., Prinn, R. G., Weiss, R. F., Tohjima, Y., Nakazawa, T., Krummel, P. B., Steele, L. P., Fraser, P., O'Doherty, S., Ishijima, K., and Aoki, S.: Nitrous oxide emissions 1999 to 2009 from a global atmospheric inversion, Atmos. Chem. Phys., 14, 1801–1817, doi:10.5194/acp-14-1801-2014, 2014a.

Thompson, R. L., Ishijima, K., Saikawa, E., Corazza, M., Karstens, U., Patra, P. K., Bergamaschi, P., Chevallier, F., Dlugokencky, E., Prinn, R. G., Weiss, R. F., O'Doherty, S., Fraser, P. J., Steele, L. P., Krummel, P. B., Vermeulen, A., Tohjima, Y., Jordan, A., Haszpra, L., Steinbacher, M., Van der Laan, S., Aalto, T., Meinhardt, F., Popa, M. E., Moncrieff, J., and Bousquet, P.: TransCom $N_2O$ model inter-comparison – Part 2: Atmospheric inversion estimates of $N_2O$ emissions, Atmos. Chem. Phys., 14, 6177–6194, doi:10.5194/acp-14-6177-2014, 2014b.

Thompson, R. L., Patra, P. K., Ishijima, K., Saikawa, E., Corazza, M., Karstens, U., Wilson, C., Bergamaschi, P., Dlugokencky, E., Sweeney, C., Prinn, R. G., Weiss, R. F., O'Doherty, S., Fraser, P. J., Steele, L. P., Krummel, P. B., Saunois, M., Chipperfield, M., and Bousquet, P.: TransCom $N_2O$ model inter-comparison – Part 1: Assessing the influence of transport and surface fluxes on tropospheric $N_2O$ variability, Atmos. Chem. Phys., 14, 4349–4368, doi:10.5194/acp-14-4349-2014, 2014c.

Thoning, K. W., Tans, P. P., and Komhyr, W. D.: Atmospheric carbon dioxide at Mauna Loa Observatory: 2. Analysis of the NOAA GMCC data, 1974–1985, J. Geophys. Res.-Atmos., 94, 8549–8565, doi:10.1029/JD094iD06p08549, 1989.





ACPD
15, 7171–7238, 2015



Tiwari, Y. K. and Kumar, K. R.: GHG observation programs in India, in: Asian GAW Greenhouse Gases Newsletter, Volume No. 3, Korea Meteorological Administration, Chungnam, South Korea, 2012.

Tiwari, Y. K., Patra, P. K., Chevallier, F., Francey, R. J., Krummel, P. B., Allison, C. E., Revadekar, J. V., Chakraborty, S., Langenfelds, R. L., Bhattacharya, S. K., Borole, D. V., Kumar, K. R., and Steele, L. P.: Carbon dioxide observations at Cape Rama, India for the period 1993–2002: implications for constraining Indian emissions, Curr. Sci. India, 101, 1562–1568, 2011.

Tiwari, Y. K., Revadekar, J. V., and Ravi Kumar, K.: Variations in atmospheric Carbon Dioxide and its association with rainfall and vegetation over India, Atmos. Environ., 68, 45–51, doi:10.1016/j.atmosenv.2012.11.040, 2013.

Tiwari, Y. K., Vellore, R. K., Ravi Kumar, K., van der Schoot, M., and Cho, C.-H.: Influence of monsoons on atmospheric $CO_2$ spatial variability and ground-based monitoring over India, Sci. Total Environ., 490, 570–578, doi:10.1016/j.scitotenv.2014.05.045, 2014.

Tohjima, Y., Maksyutov, S., Machida, T., and Inoue, G.: Airborne measurements of atmospheric methane over oil fields in western Siberia, Geophys. Res. Lett., 23, 1621–1624, doi:10.1029/96gl01027, 1996.

Turnbull, J. C., Miller, J. B., Lehman, S. J., Tans, P. P., Sparks, R. J., and Southon, J.: Comparison of $14CO_2$, CO, and SF6 as tracers for recently added fossil fuel $CO_2$ in the atmosphere and implications for biological $CO_2$ exchange, Geophys. Res. Lett., 33, L01817, doi:10.1029/2005gl024213, 2006.

Valsala, V., Tiwari, Y. K., Pillai, P., Roxy, M., Maksyutov, S., and Murtugudde, R.: Intraseasonal variability of terrestrial biospheric $CO_2$ fluxes over India during summer monsoons, J. Geophys. Res.-Biogeo., 118, 752–769, doi:10.1002/jgrg.20037, 2013.

van der Werf, G. R., Randerson, J. T., Giglio, L., Collatz, G. J., Kasibhatla, P. S., and Arellano Jr., A. F.: Interannual variability in global biomass burning emissions from 1997 to 2004, Atmos. Chem. Phys., 6, 3423–3441, doi:10.5194/acp-6-3423-2006, 2006.

van der Werf, G. R., Randerson, J. T., Giglio, L., Collatz, G. J., Mu, M., Kasibhatla, P. S., Morton, D. C., DeFries, R. S., Jin, Y., and van Leeuwen, T. T.: Global fire emissions and the contribution of deforestation, savanna, forest, agricultural, and peat fires (1997–2009), Atmos. Chem. Phys., 10, 11707–11735, doi:10.5194/acp-10-11707-2010, 2010.





ACPD
15, 7171–7238, 2015



Venkataraman, C., Habib, G., Eiguren-Fernandez, A., Miguel, A. H., and Friedlander, S. K.: Residential biofuels in South Asia: carbonaceous aerosol emissions and climate impacts, Science, 307, 1454–1456, 2005.

Volk, C. M., Elkins, J. W., Fahey, D. W., Dutton, G. S., Gilligan, J. M., Loewenstein, M., Podolske, J. R., Chan, K. R., and Gunson, M. R.: Evaluation of source gas lifetimes from stratospheric observations, J. Geophys. Res.-Atmos., 102, 25543–25564, doi:10.1029/97jd02215, 1997.

Wada, A., Matsueda, H., Sawa, Y., Tsuboi, K., and Okubo, S.: Seasonal variation of enhancement ratios of trace gases observed over 10 years in the western North Pacific, Atmos. Environ., 45, 2129–2137, doi:10.1016/j.atmosenv.2011.01.043, 2011.

Wang, R., Tao, S., Ciais, P., Shen, H. Z., Huang, Y., Chen, H., Shen, G. F., Wang, B., Li, W., Zhang, Y. Y., Lu, Y., Zhu, D., Chen, Y. C., Liu, X. P., Wang, W. T., Wang, X. L., Liu, W. X., Li, B. G., and Piao, S. L.: High-resolution mapping of combustion processes and implications for $CO_2$ emissions, Atmos. Chem. Phys., 13, 5189–5203, doi:10.5194/acp-13-5189-2013, 2013.

Xiao, Y., Jacob, D. J., Wang, J. S., Logan, J. A., Palmer, P. I., Suntharalingam, P., Yantosca, R. M., Sachse, G. W., Blake, D. R., and Streets, D. G.: Constraints on Asian and European sources of methane from $CH_4$-$C_2H_6$-CO correlations in Asian outflow, J. Geophys. Res.-Atmos., 109, D15S16, doi:10.1029/2003jd004475, 2004.

Xiong, X., Houweling, S., Wei, J., Maddy, E., Sun, F., and Barnet, C.: Methane plume over south Asia during the monsoon season: satellite observation and model simulation, Atmos. Chem. Phys., 9, 783–794, doi:10.5194/acp-9-783-2009, 2009.

Yan, X., Cai, Z., Ohara, T., and Akimoto, H.: Methane emission from rice fields in mainland China: amount and seasonal and spatial distribution, J. Geophys. Res.-Atmos., 108, 4505, doi:10.1029/2002jd003182, 2003.

Yashiro, H., Sudo, K., Yonemura, S., and Takigawa, M.: The impact of soil uptake on the global distribution of molecular hydrogen: chemical transport model simulation, Atmos. Chem. Phys., 11, 6701–6719, doi:10.5194/acp-11-6701-2011, 2011.

Yevich, R. and Logan, J. A.: An assessment of biofuel use and burning of agricultural waste in the developing world, Global Biogeochem. Cy., 17, 1095, doi:10.1029/2002gb001952, 2003.

Yver, C.: Estimation des sources et puits du dihydrogène troposphérique – développements instrumentaux, mesures atmosphériques et assimilation variationnelle, Ph.D. dissertation, Université de Versailles, Saint Quentin, 2010.





ACPD
15, 7171–7238, 2015



Yver, C., Schmidt, M., Bousquet, P., Zahorowski, W., and Ramonet, M.: Estimation of the molecular hydrogen soil uptake and traffic emissions at a suburban site near Paris through hydrogen, carbon monoxide, and radon-222 semicontinuous measurements, J. Geophys. Res.-Atmos., 114, D18304, doi:10.1029/2009jd012122, 2009.

Yver, C. E., Pison, I. C., Fortems-Cheiney, A., Schmidt, M., Chevallier, F., Ramonet, M., Jordan, A., Søvde, O. A., Engel, A., Fisher, R. E., Lowry, D., Nisbet, E. G., Levin, I., Hammer, S., Necki, J., Bartyzel, J., Reimann, S., Vollmer, M. K., Steinbacher, M., Aalto, T., Maione, M., Arduini, J., O'Doherty, S., Grant, A., Sturges, W. T., Forster, G. L., Lunder, C. R., Privalov, V., Paramonova, N., Werner, A., and Bousquet, P.: A new estimation of the recent tropospheric molecular hydrogen budget using atmospheric observations and variational inversion, Atmos. Chem. Phys., 11, 3375–3392, doi:10.5194/acp-11-3375-2011, 2011.

Zhang, F., Zhou, L. X., Novelli, P. C., Worthy, D. E. J., Zellweger, C., Klausen, J., Ernst, M., Steinbacher, M., Cai, Y. X., Xu, L., Fang, S. X., and Yao, B.: Evaluation of in situ measurements of atmospheric carbon monoxide at Mount Waliguan, China, Atmos. Chem. Phys., 11, 5195–5206, doi:10.5194/acp-11-5195-2011, 2011.

Zhang, H. F., Chen, B. Z., van der Laan-Luijk, I. T., Machida, T., Matsueda, H., Sawa, Y., Fukuyama, Y., Langenfelds, R., van der Schoot, M., Xu, G., Yan, J. W., Cheng, M. L., Zhou, L. X., Tans, P. P., and Peters, W.: Estimating Asian terrestrial carbon fluxes from CONTRAIL aircraft and surface $CO_2$ observations for the period 2006–2010, Atmos. Chem. Phys., 14, 5807–5824, doi:10.5194/acp-14-5807-2014, 2014.

Zhang, X. I. A., Nakazawa, T., Ishizawa, M., Aoki, S., Nakaoka, S.-I., Sugawara, S., Maksyutov, S., Saeki, T., and Hayasaka, T.: Temporal variations of atmospheric carbon dioxide in the southernmost part of Japan, Tellus B, 59, 654–663, doi:10.1111/j.1600-0889.2007.00288.x, 2007.

Zhao, C. L. and Tans, P. P.: Estimating uncertainty of the WMO mole fraction scale for carbon dioxide in air, J. Geophys. Res.-Atmos., 111, D08S09, doi:10.1029/2005jd006003, 2006.





ACPD
15, 7171–7238, 2015



**Table 1.** Annual mean values and average peak-to-peak amplitudes of trace gases at HLE, PON, PBL and the two additional NOAA/ESRL stations – KZM and WLG. For each species at each station, the annual mean values and average peak-to-peak amplitude are calculated from the smoothed curve and mean season cycle, respectively. Uncertainty of each estimate is calculated from 1 SD of 1000 bootstrap replicates.

| | HLE | PON | PBL | KZM | WLG |
|---|---|---|---|---|---|
| $CO_2$ (ppm) | | | | | |
| Annual mean 2007 | 382.3 ± 0.3 | 386.6 ± 0.9 | – | 382.7 ± 0.2 | 384.2 ± 0.2 |
| Annual mean 2008 | 384.6 ± 0.5 | 388.1 ± 0.9 | – | 385.7 ± 0.2 | 386.0 ± 0.2 |
| Annual mean 2009 | 387.2 ± 0.2 | 389.0 ± 0.6 | – | – | 387.4 ± 0.2 |
| Annual mean 2010 | 389.4 ± 0.1 | 391.3 ± 1.5 | 387.6 ± 0.7 | – | 390.1 ± 0.2 |
| Annual mean 2011 | 391.4 ± 0.3 | – | 390.2 ± 0.6 | – | 392.2 ± 0.2 |
| Trend | 2.1 ± 0.0 | 1.7 ± 0.1 | – | – | 2.0 ± 0.0 |
| RSD | 0.7 | 4.0 | 1.5 | 1.5 | 1.4 |
| Amplitude | 8.2 ± 0.4 | 7.6 ± 1.4 | 11.1 ± 1.3 | 13.8 ± 0.5 | 11.1 ± 0.4 |
| $D_{max}$ | 122.0 ± 2.9 | 111.0 ± 13.4 | 97.0 ± 26.0 | 75.0 ± 2.6 | 100.0 ± 1.5 |
| $D_{min}$ | 261.0 ± 3.0 | 327.0 ± 54.3 | 242.0 ± 7.7 | 205.0 ± 2.1 | 222.0 ± 1.6 |
| $CH_4$ (ppb) | | | | | |
| Annual mean 2007 | 1814.8 ± 2.9 | 1859.2 ± 6.7 | – | 1842.6 ± 2.4 | 1841.0 ± 1.8 |
| Annual mean 2008 | 1833.1 ± 5.4 | 1856.1 ± 10.4 | – | 1856.6 ± 2.3 | 1845.6 ± 1.5 |
| Annual mean 2009 | 1830.2 ± 1.7 | 1865.7 ± 5.1 | – | – | 1851.8 ± 1.9 |
| Annual mean 2010 | 1830.5 ± 2.1 | 1876.9 ± 9.1 | 1867.5 ± 15.4 | – | 1857.6 ± 1.4 |
| Annual mean 2011 | 1849.5 ± 5.2 | – | 1852.0 ± 7.6 | – | 1859.9 ± 1.2 |
| Trend | 4.9 ± 0.0 | 9.4 ± 0.1 | – | – | 5.3 ± 0.0 |
| RSD | 9.1 | 34.4 | 22.4 | 14.6 | 12.3 |
| Amplitude | 28.9 ± 4.2 | 124.1 ± 10.2 | 143.9 ± 12.4 | 22.7 ± 4.7 | 17.5 ± 2.2 |
| $D_{max}$ | 219.0 ± 4.6 | 337.0 ± 6.1 | 345.0 ± 87.6 | 236.0 ± 43.2 | 222.0 ± 6.2 |
| $D_{min}$ | 97.0 ± 58.9 | 189.0 ± 10.7 | 193.0 ± 13.5 | 338.0 ± 39.0 | 340.0 ± 96.6 |
| $N_2O$ (ppb) | | | | | |
| Annual mean 2007 | 322.2 ± 0.1 | 324.8 ± 0.3 | – | | |
| Annual mean 2008 | 322.9 ± 0.1 | 326.3 ± 0.3 | – | | |
| Annual mean 2009 | 323.5 ± 0.1 | 326.7 ± 0.3 | – | | |
| Annual mean 2010 | 324.0 ± 0.1 | 327.1 ± 0.5 | 329.0 ± 0.5 | | |
| Annual mean 2011 | 325.2 ± 0.1 | – | 327.9 ± 0.3 | | |
| Trend | 0.8 ± 0.0 | 0.8 ± 0.1 | – | | |
| RSD | 0.3 | 1.4 | 1.1 | | |
| Amplitude | 0.6 ± 0.1 | 1.2 ± 0.5 | 2.2 ± 0.6 | | |
| $D_{max}$ | 227.0 ± 11.8 | 262.0 ± 83.2 | 313.0 ± 42.6 | | |
| $D_{min}$ | 115.0 ± 16.4 | 141.0 ± 48.2 | 65.0 ± 33.4 | | |





ACPD
15, 7171–7238, 2015



**Table 1.** Continued.

| | HLE | PON | PBL | KZM | WLG |
|---|---|---|---|---|---|
| $SF_6$ (ppt) | | | | | |
| Annual mean 2007 | 6.26 ± 0.03 | 6.19 ± 0.01 | – | | |
| Annual mean 2008 | 6.54 ± 0.03 | 6.49 ± 0.02 | – | | |
| Annual mean 2009 | 6.79 ± 0.01 | 6.77 ± 0.01 | – | | |
| Annual mean 2010 | 7.17 ± 0.01 | 7.08 ± 0.02 | 7.10 ± 0.07 | | |
| Annual mean 2011 | 7.38 ± 0.01 | – | 7.45 ± 0.03 | | |
| Trend | 0.29 ± 0.05 | 0.31 ± 0.05 | – | | |
| RSD | 0.07 | 0.05 | 0.12 | | |
| Amplitude | 0.15 ± 0.03 | 0.24 ± 0.02 | 0.48 ± 0.07 | | |
| $D_{max}$ | 320.0 ± 8.3 | 327.0 ± 12.1 | 342.0 ± 59.9 | | |
| $D_{min}$ | 211.0 ± 65.1 | 204.0 ± 3.3 | 210.0 ± 18.1 | | |
| CO (ppb) | | | | | |
| Annual mean 2007 | 104.7 ± 1.4 | 200.5 ± 7.8 | – | 121.7 ± 1.7 | 141.0 ± 4.3 |
| Annual mean 2008 | 103.1 ± 2.1 | 175.3 ± 13.1 | – | 123.7 ± 1.7 | 129.0 ± 2.9 |
| Annual mean 2009 | 98.9 ± 1.9 | 174.3 ± 4.8 | – | – | 131.9 ± 3.7 |
| Annual mean 2010 | 99.0 ± 1.2 | 185.1 ± 8.7 | 157.6 ± 20.4 | – | 130.2 ± 3.9 |
| Annual mean 2011 | 99.4 ± 2.2 | – | 145.9 ± 9.9 | – | 124.0 ± 2.3 |
| Trend | −2.2 ± 0.0 | 0.4 ± 0.1 | – | – | −1.9 ± 0.0 |
| RSD | 6.5 | 32.0 | 30.8 | 11.8 | 22.5 |
| Amplitude | 28.4 ± 2.3 | 78.2 ± 11.6 | 144.1 ± 16.0 | 37.1 ± 4.4 | 38.6 ± 5.1 |
| $D_{max}$ | 79.0 ± 11.4 | 4.0 ± 160.2 | 12.0 ± 117.9 | 72.0 ± 5.0 | 94.0 ± 38.2 |
| $D_{min}$ | 297.0 ± 5.3 | 238.0 ± 46.1 | 213.0 ± 23.0 | 318.0 ± 6.1 | 331.0 ± 6.2 |
| $H_2$ (ppb) | | | | | |
| Annual mean 2007 | 539.6 ± 2.1 | 574.5 ± 2.4 | – | 502.4 ± 2.0 | 500.9 ± 1.5 |
| Annual mean 2008 | 533.2 ± 3.2 | 558.2 ± 5.3 | – | – | – |
| Annual mean 2009 | 533.3 ± 1.6 | 562.4 ± 1.6 | – | – | – |
| Annual mean 2010 | 533.5 ± 1.8 | 563.9 ± 2.3 | 558.6 ± 2.4 | – | – |
| Annual mean 2011 | 536.9 ± 1.5 | – | 555.4 ± 1.6 | – | – |
| Trend | −0.5 ± 0.0 | −1.3 ± 0.1 | – | – | – |
| RSD | 6.6 | 8.4 | 7.0 | 13.3 | 9.5 |
| Amplitude | 15.8 ± 2.2 | 21.6 ± 3.4 | 21.3 ± 5.0 | 16.7 ± 4.0 | 22.8 ± 3.0 |
| $D_{max}$ | 120.0 ± 8.7 | 96.0 ± 9.6 | 99.0 ± 8.8 | 120.0 ± 34.2 | 51.0 ± 13.4 |
| $D_{min}$ | 266.0 ± 39.6 | 219.0 ± 10.3 | 353.0 ± 87.8 | 341.0 ± 78.3 | 298.0 ± 6.5 |

Abbreviations: RSD – residual SD; $D_{max}$ – the Julian day corresponding to the maximum of the mean seasonal cycle; $D_{min}$ – the Julian day corresponding to the minimum of the mean seasonal cycle.





ACPD
15, 7171–7238, 2015



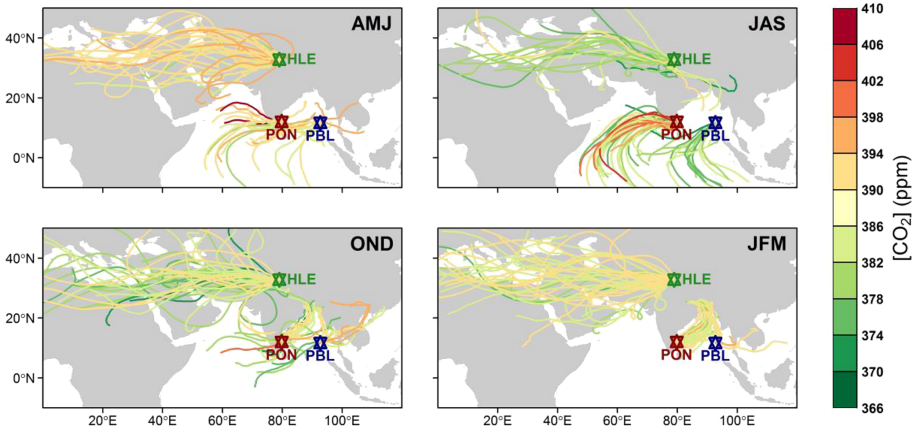


**Figure 1.** Five-day back-trajectories calculated for all sampling dates over the period 2007–2011 at Hanle (HLE), Pondicherry (PON), and Port Blair (PBL) during April–June (AMJ), July–September (JAS), October–December (OND) and January–March (JFM), respectively. Back-trajectories are colored according to individual $CO_2$ measurements on the corresponding sampling dates.





ACPD
15, 7171–7238, 2015



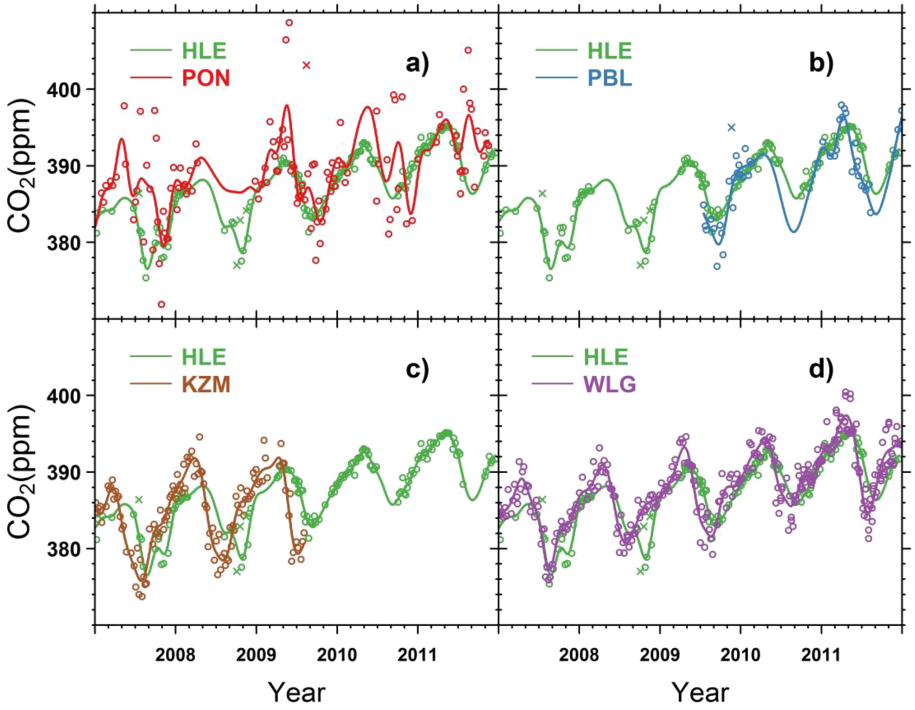


**Figure 2.** Time series of $CO_2$ flask measurements at **(a)** HLE and PON, **(b)** HLE and PBL, **(c)** HLE and KZM, and **(d)** HLE and WLG. "∘" denotes flask data used to fit the smoothed curves, while "× " denotes discarded flask data lying outside 3 times the residual SDs from the smoothed curve fits. For each station, the smoothed curve is fitted using Thoning's method (Thoning et al., 1989) after removing outliers.





ACPD
15, 7171–7238, 2015



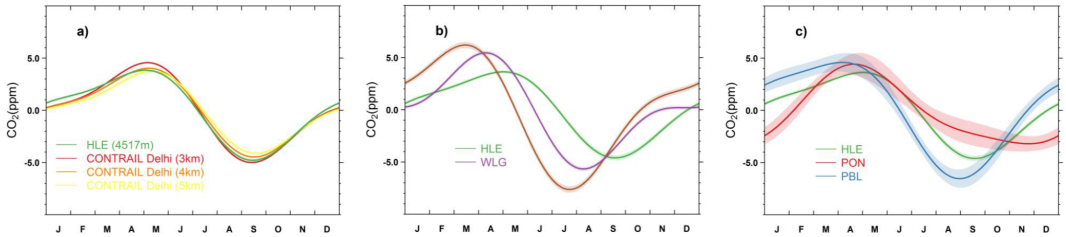


**Figure 3. (a)** The mean $CO_2$ seasonal cycle at HLE, in comparison with the mean seasonal cycles derived from the in-situ $CO_2$ measurements over New Delhi at different altitude bands (3–4 km, 4–5 km, and 5–6 km) by the CONTRAIL project (2006–2010). **(b)** The mean $CO_2$ seasonal cycles at HLE, KZM and WLG. **(c)** The mean $CO_2$ seasonal cycles at HLE, PON and PBL. For each station, the mean seasonal cycle is calculated based on the curve fitting procedures of $CO_2$ flask data. Shaded area indicates the uncertainty of the mean seasonal cycle calculated from 1 SD of 1000 bootstrap replicates. For the CONTRAIL datasets, $CO_2$ measurements over New Delhi were first averaged by altitude bands. A fitting procedure was then applied to the aggregated $CO_2$ measurements to generate the mean season cycle for different altitude bands.





ACPD
15, 7171–7238, 2015



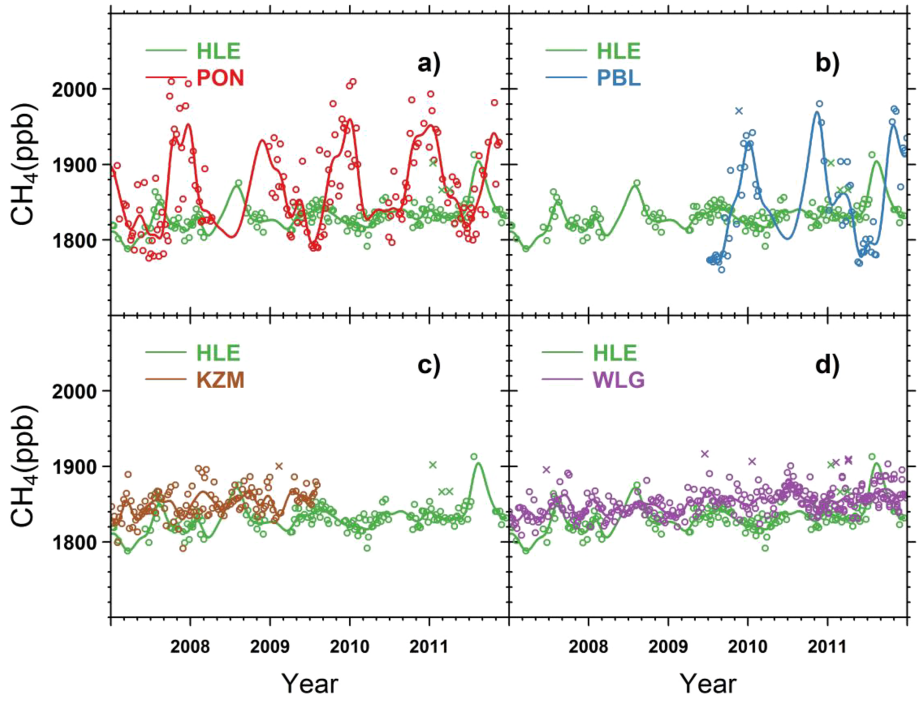


**Figure 4.** Same as Fig. 2, but for $CH_4$.





ACPD
15, 7171–7238, 2015



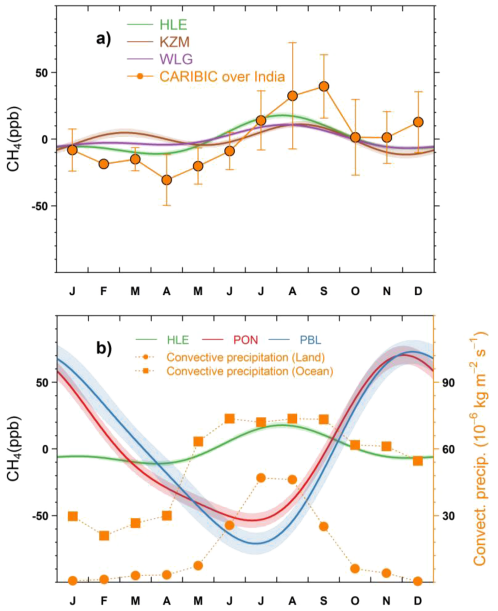


**Figure 5.** The mean $CH_4$ seasonal cycles observed at **(a)** HLE, KZM and WLG, **(b)** HLE, PON and PBL. For each station, the mean seasonal cycle is calculated based on the curve fitting procedures of $CH_4$ flask data. Shaded area indicates the uncertainty of the mean seasonal cycle calculated from 1 SD of 1000 bootstrap replicates. The mean $CH_4$ seasonal cycle derived from aircraft flask measurements in the upper troposphere (200–300 hPa) over the Indian subcontinent (10–35° N, 60–100° E) by the CARIBIC project is also shown in **(a)**. The CARIBIC flask measurements over the years 2005–2008 and 2011–2012 are averaged by month to generate the mean seasonal cycle. The error bars indicate 1 SD of $CH_4$ flask measurements within the month. To indicate the intensity of deep convection, we also plot the monthly convective precipitation averaged during 2006–2010 over the Indian subcontinent (land grids within 10–35° N, 70–90° E) and Indian Ocean (ocean grids within 0–30° N, 50–100° E). The dataset of convective precipitation is derived from an LMDz simulation nudged with ECMWF reanalysis datasets.





ACPD
15, 7171–7238, 2015



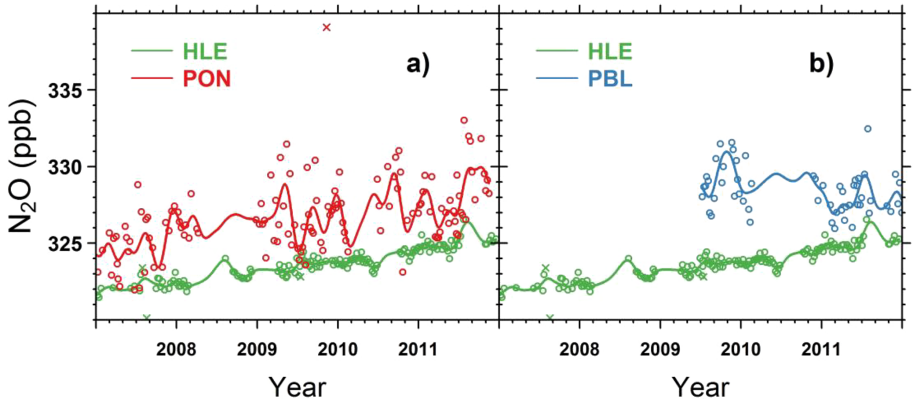


**Figure 6.** Time series of $N_2O$ flask measurements at **(a)** HLE and PON, **(b)** HLE and PBL. "∘" denotes flask data used to fit the smoothed curves, while "× " denotes discarded flask data lying outside 3 times the residual SDs from the smoothed curve fits. For each station, the smoothed curve is fitted using Thoning's method (Thoning et al., 1989) after removing outliers.





ACPD
15, 7171–7238, 2015



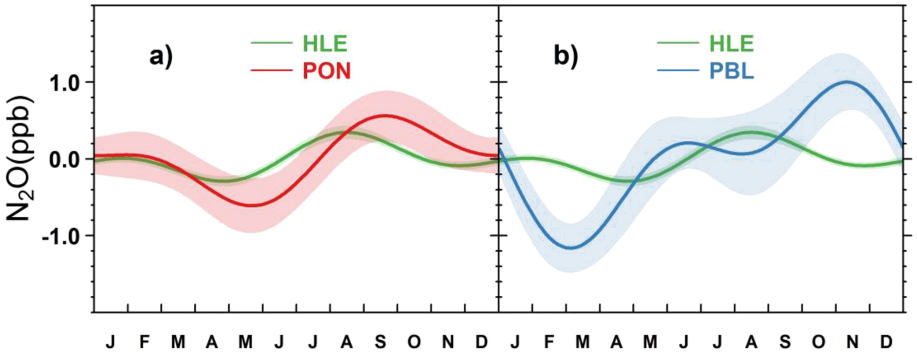


**Figure 7.** The mean $N_2O$ seasonal cycles observed at **(a)** HLE and PON, **(b)** HLE and PBL. For each station, the mean seasonal cycle is calculated based on the curve fitting procedures of $N_2O$ flask data. Shaded area indicates the uncertainty of the mean seasonal cycle calculated from 1 SD of 1000 bootstrap replicates.





ACPD
15, 7171–7238, 2015



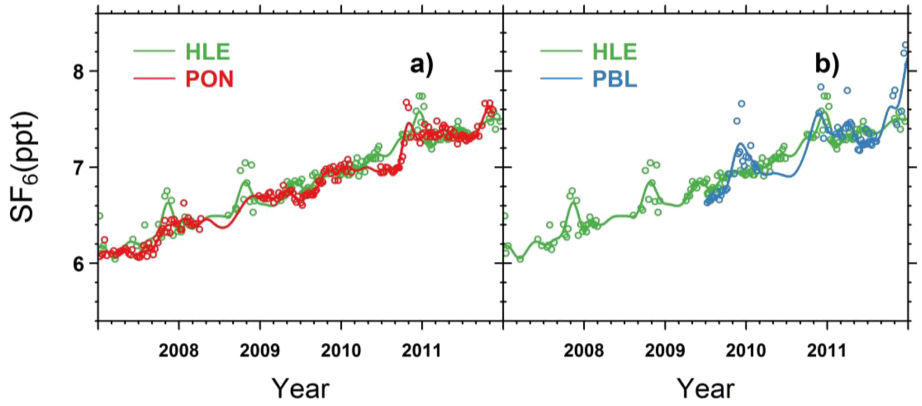


**Figure 8.** Same as Fig. 6, but for $SF_6$.





ACPD
15, 7171–7238, 2015



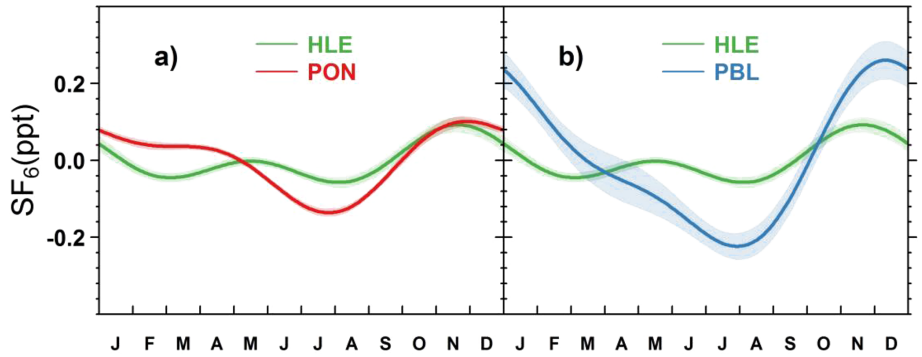


**Figure 9.** Same as Fig. 7, but for $SF_6$.





ACPD
15, 7171–7238, 2015



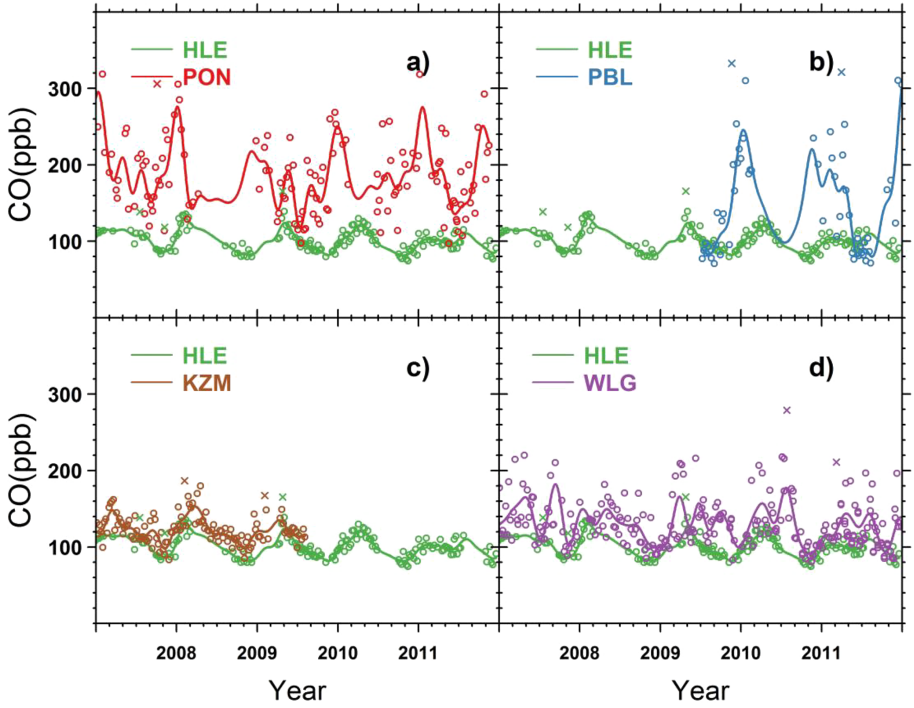


**Figure 10.** Same as Fig. 2, but for CO.





ACPD
15, 7171–7238, 2015



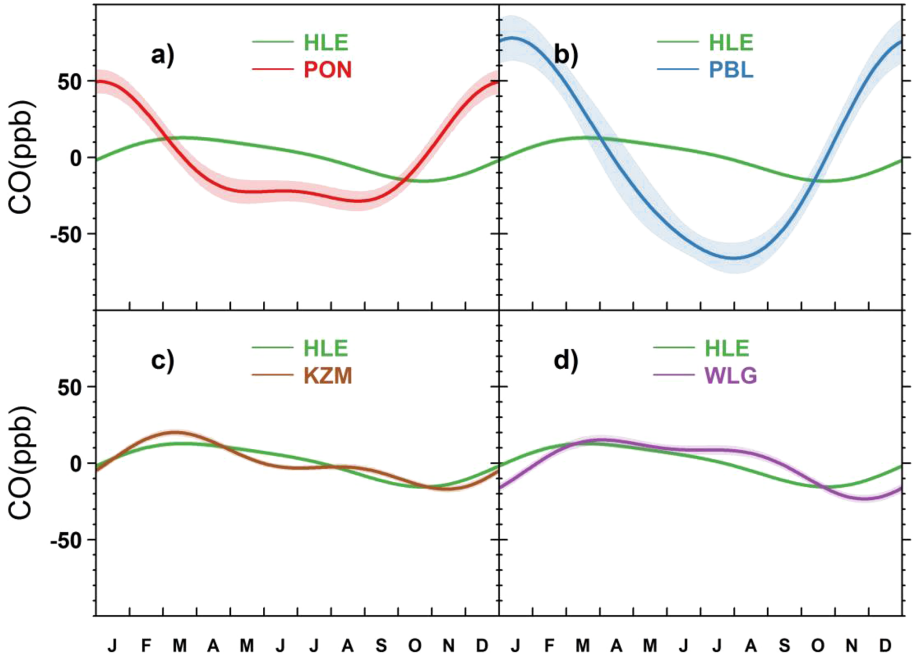


**Figure 11.** The mean CO seasonal cycles observed at **(a)** HLE and PON, **(b)** HLE and PBL, **(c)** HLE and KZM, and **(d)** HLE and WLG. For each station, the mean seasonal cycle is calculated based on the curve fitting procedures of CO flask data. Shaded area indicates the uncertainty of the mean seasonal cycle calculated from 1 SD of 1000 bootstrap replicates.





ACPD
15, 7171–7238, 2015



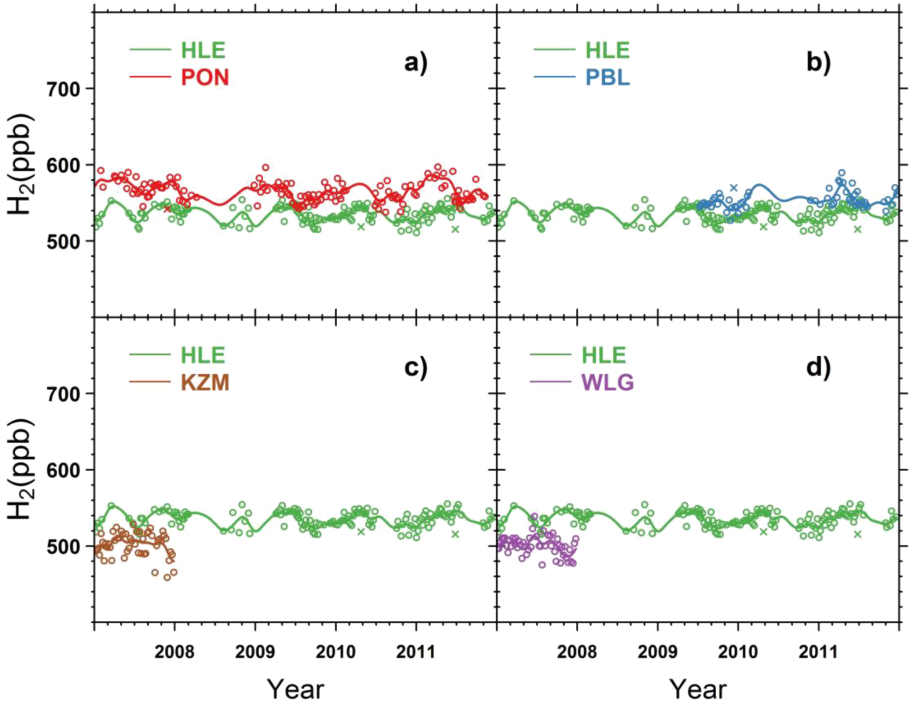


**Figure 12.** Same as Fig. 2, but for $H_2$.





ACPD
15, 7171–7238, 2015



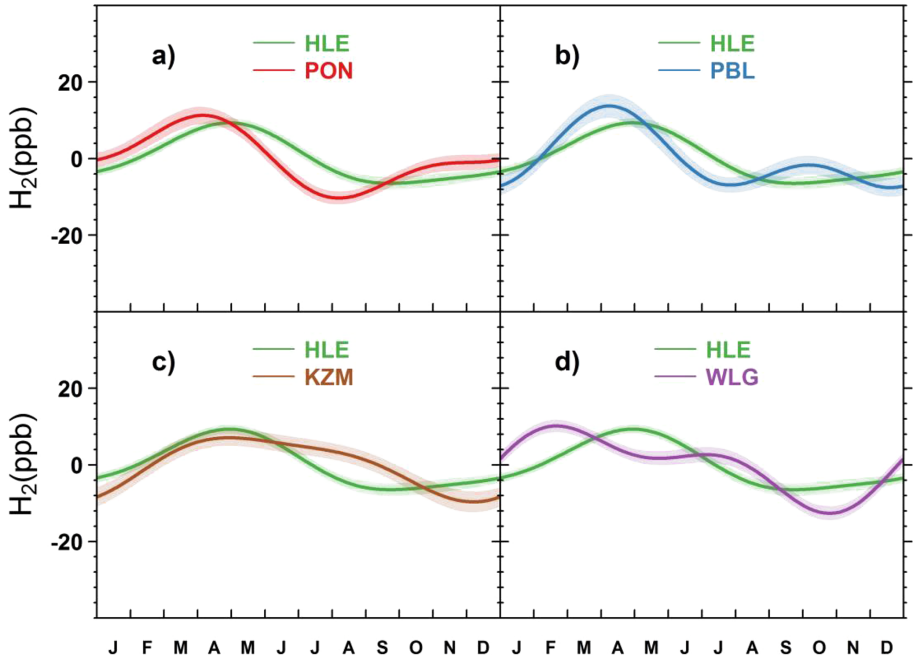


**Figure 13.** Same as Fig. 11, but for $H_2$.





ACPD
15, 7171–7238, 2015



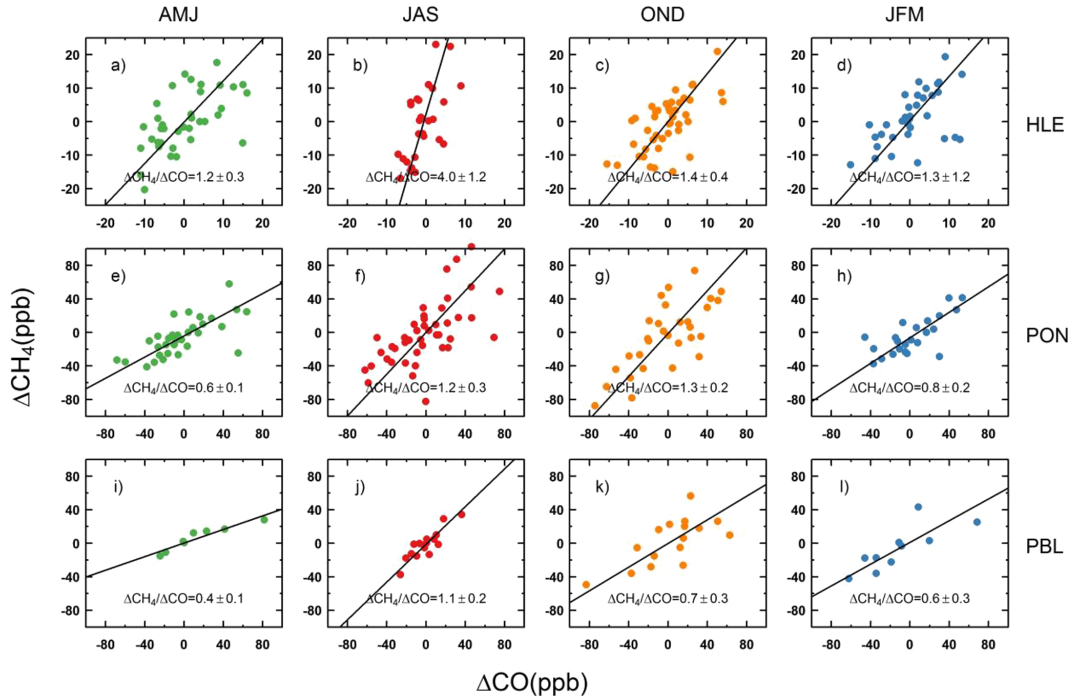


**Figure 14.** The relationships between $\Delta CH_4$ and $\Delta CO$ at HLE **(a–d)**, PON **(e–h)**, and PBL **(i–l)** for April–June (AMJ), July–September (JAS), October–December (OND), and January–March (JFM). For each panel, $\Delta CH_4$ and $\Delta CO$ are estimated as residuals from smoothed curves. The $\Delta CH_4/\Delta CO$ ratio is the slope of the fitting line from the orthogonal distance regression, with the SD calculated from 1000 bootstrap replications.





ACPD
15, 7171–7238, 2015



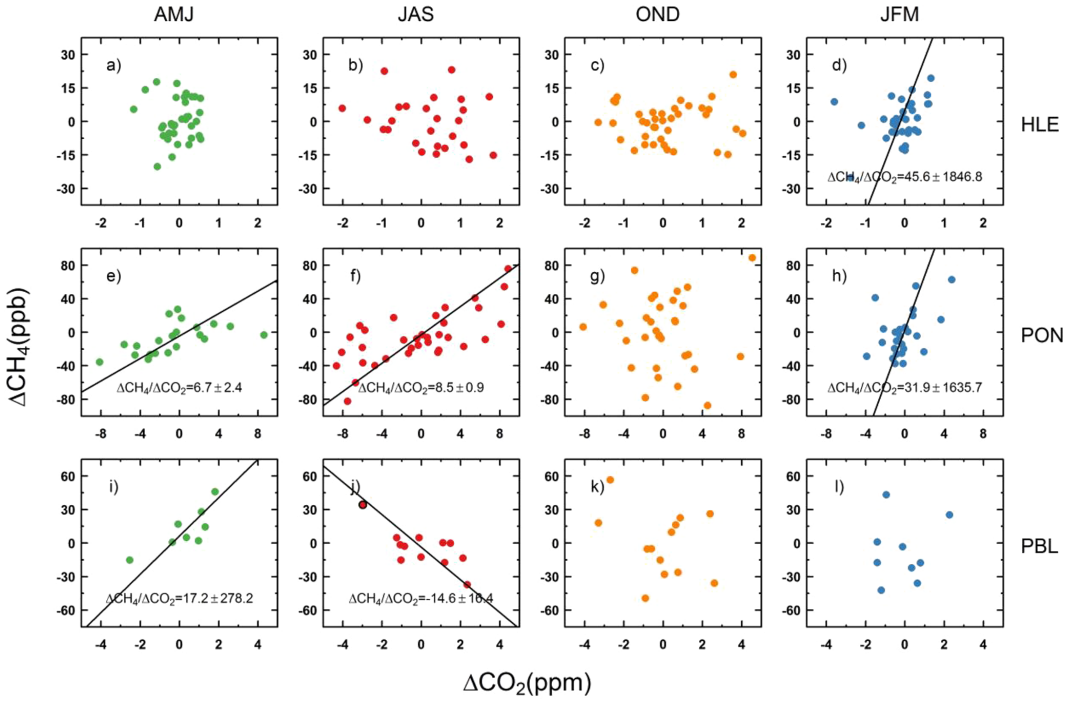


**Figure 15.** Same as Fig. 14, but for the relationships between $\Delta CH_4$ and $\Delta CO_2$. For $\Delta CH_4$ and $\Delta CO_2$ that is not significantly correlated, the fitting line is not plotted.





ACPD
15, 7171–7238, 2015



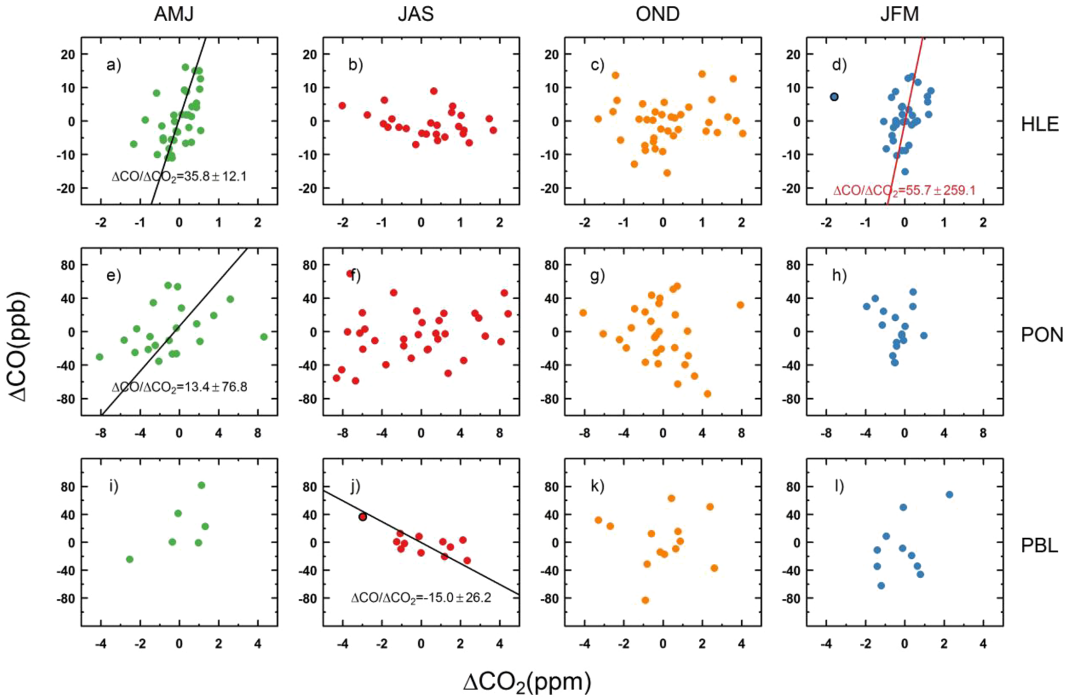


**Figure 16.** Same as Fig. 14, but for the relationships between ΔCO and $\Delta CO_2$. For ΔCO and $\Delta CO_2$ that is not significantly correlated, the fitting line is usually not plotted.





ACPD
15, 7171–7238, 2015



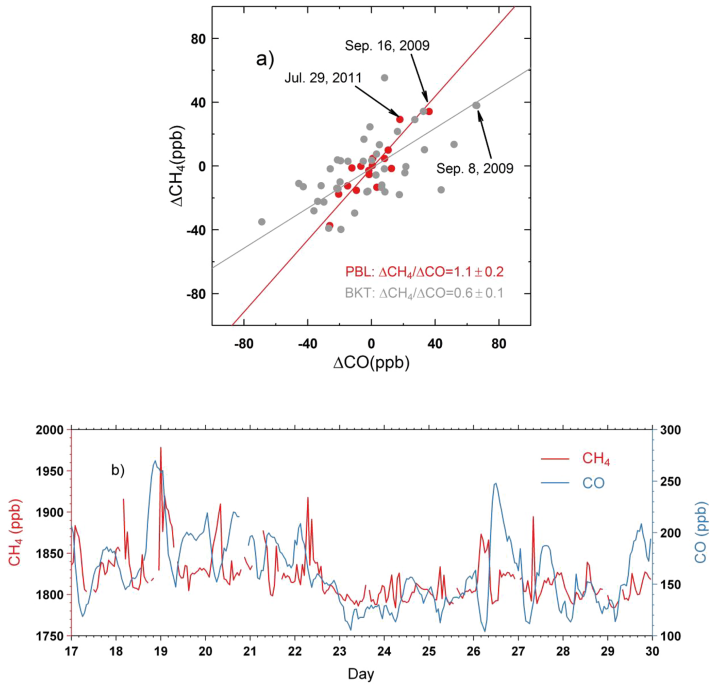


**Figure 17. (a)** The relationship between $\Delta CH_4$ and $\Delta CO$ at PBL (colored by red) and BKT (colored by grey) during July–September (JAS) over the period of 2007–2011. $\Delta CH_4$ and $\Delta CO$ are estimated as residuals from smoothed curves. The $\Delta CH_4/\Delta CO$ ratio is the slope of the fitting line from orthogonal distance regression (ODR), with the SD calculated from 1000 bootstrap replications. Two abnormal events at PBL are labeled, with enhancements of $CH_4$ and CO on 16 September 2009 and 29 July 2011, respectively. Enhancements of $CH_4$ and CO are also observed at BKT on 8 September 2009. **(b)** Hourly $CH_4$ and CO measurements at BKT in July 2011 (BMKG & EMPA). Enhancements of $CH_4$ and CO are observed during 17–21 July 2011.





ACPD
15, 7171–7238, 2015